CMI

www.nature.com/cmi

ARTICLE

Check for updates

NAD^+ salvage governs the immunosuppressive capacity of mesenchymal stem cells

Jiankai Fang[1], Pengbo Hou[1,2], Shisong Liu[1], Muqiu Zuo[1], Zhanhong Liu[1,2], Wangwang Chen[3], Yuyi Han[1,2], Yanan Li[1,2], Tingting Wang[1], Chao Feng[1,2], Peishan Li[1], Changshun Shao[1]✉ and Yufang Shi[1,4]✉

Mesenchymal stem/stromal cells (MSCs) possess robust immunoregulatory functions and are promising therapeutics for inflammatory disorders. This capacity is not innate but is activated or 'licensed' by inflammatory cytokines. The licensing mechanism remains unclear. Here, we examined whether inflammatory cytokines metabolically reprogrammed MSCs to confer this immunoregulatory capacity. In response to stimulation by inflammatory cytokines, MSCs exhibited a dramatic increase in the consumption of glucose, which was accompanied by an enhanced use of nicotinamide adenine dinucleotide (NAD^+) and increased expression of nicotinamide phosphoribosyltransferase (NAMPT), a central enzyme in the salvage pathway for NAD^+ production. When NAD^+ synthesis was blocked by inhibiting or depleting NAMPT, the immunosuppressive function of MSCs induced by inflammatory cytokines was greatly attenuated. Consequently, when NAD^+ metabolism in MSCs was perturbed, their therapeutic benefit was decreased in mice suffering from inflammatory bowel disease and acute liver injury. Further analysis revealed that NAMPT-driven production of NAD^+ was critical for the inflammatory cytokine-induced increase in glycolysis in MSCs. Furthermore, the increase in glycolysis led to succinate accumulation in the tricarboxylic acid cycle, which led to hypoxia-inducible factor 1α (HIF-1α) stabilization and subsequently increased the transcription of key glycolytic genes, thereby persistently maintaining glycolytic flux. This study demonstrated that unlike its proinflammatory role in immune cells, NAD^+ metabolism governs the anti-inflammatory function of MSCs during inflammation.

Keywords: Mesenchymal stem/stromal cells; NAD^+ metabolism; Immunomodulation; Glycolysis; HIF-1α; Succinate

Cellular & Molecular Immunology (2023) 20:1171–1185; https://doi.org/10.1038/s41423-023-01073-2

INTRODUCTION

Mesenchymal stem cells (MSCs), which are a population of tissue stem cells in almost all tissues, can differentiate into adipocytes, osteoblasts and chondrocytes [1–3]. Beyond the perceived replacement of damaged cells, MSCs orchestrate local and systemic innate and adaptive immune responses through the release of various immunoregulatory factors, which makes them highly effective in treating many autoimmune and hyperinflammatory disorders, such as graft-versus-host disease (GvHD), multiple sclerosis (MS), systemic lupus erythematosus (SLE), and inflammatory bowel disease (IBD) [4–8].

The inflamed tissue microenvironment critically shapes the immunoregulatory properties of MSCs. MSCs activated by appropriate inflammatory cues, such as interferon-γ (IFN-γ) with tumor necrosis factor-α (TNF-α) or interleukin-1 (IL-1), can express large amounts of inducible nitric oxide synthase (iNOS) in rodents (indoleamine-2,3-dioxygenase, or IDO, in humans and non-rodent mammalian species) and chemokines, particularly the ligands of the T-cell-specific chemokine receptors CC-chemokine receptor 5 (CCR5) and CXC-chemokine receptor 3 (CXCR3). In this scenario, immune cells are recruited to the vicinity of MSCs and are subsequently inhibited by nitric oxide (NO) [9, 10]. In addition, inflammatory cytokine-primed MSCs can reprogram lipopolysaccharide (LPS)-stimulated macrophages toward anti-inflammatory phenotypes by releasing prostaglandin E_2 (PGE_2) [11]. Although several preclinical and clinical studies have demonstrated that MSC-mediated immunomodulation requires inflammatory cytokines, the underlying mechanisms, especially metabolic requirements, have yet to be characterized.

Nicotinamide adenine dinucleotide (NAD^+) not only functions as an essential cofactor in cellular bioenergetics but also acts as an indispensable cosubstrate for NAD^+-consuming enzymes, such as sirtuins, poly(ADP-ribose) polymerases (PARPs) and cyclic ADP-ribose (cADPR) synthetases. NAD^+ is required for approximately 500 different enzymatic reactions in almost all known biological processes [12–17]. Intracellular NAD^+ levels reflect the balance between NAD^+ consumption and net biosynthesis via three discrete pathways: the de novo biosynthetic pathway, the Preiss-Handler pathway, and the salvage pathway [12–18]. In mammals, the NAD^+ salvage pathway is primarily responsible for NAD^+

[1]The Third Affiliated Hospital of Soochow University, Institutes for Translational Medicine, State Key Laboratory of Radiation Medicine and Protection, Suzhou Medical College of Soochow University, Suzhou, China. [2]Department of Experimental Medicine and Biochemical Sciences, TOR, University of Rome "Tor Vergata", Rome, Italy. [3]Laboratory Animal Center, Suzhou Medical College of Soochow University, Suzhou, China. [4]Shanghai Institute of Nutrition and Health, Chinese Academy of Sciences, Shanghai, China.
✉email: shaoc@suda.edu.cn; yfshi@suda.edu.cn

Received: 3 April 2023 Accepted: 24 July 2023
Published online: 14 August 2023

production [19, 20]. In this context, the rate of NAD^+ synthesis is largely limited by the first step of the salvage pathway, in which nicotinamide (NAM) is converted to nicotinamide mononucleotide (NMN) by NAM phosphoribosyltransferase (NAMPT) [21]. Dynamic NAMPT levels fluctuate in response to NAD^+ demands and intrinsic cellular stresses under inflammatory conditions, such as type 2 diabetes mellitus (T2DM), rheumatoid arthritis (RA), and IBD [22–24].

In the present study, we investigated the role of NAD^+ dynamics in the acquisition of immunomodulatory capabilities in MSCs in response to inflammatory priming. We found that intracellular NAD^+ levels in MSCs were dramatically decreased in response to inflammatory stimulation. Detailed analysis demonstrated that the NAD^+ salvage pathway was crucial for the immunosuppressive properties of MSCs. Inhibition or depletion of NAMPT, a key enzyme in the NAD^+ salvage pathway, abrogated the expression of chemokines and immunosuppressive factors and thus decreased the therapeutic efficacy of MSCs in mouse models of inflammatory conditions. Mechanistically, inhibiting NAMPT activity disrupted aerobic glycolysis and the subsequent immunoregulatory functions of MSCs. Interestingly, an increase in NAMPT-dependent glycolysis was accompanied by the accumulation of succinate, an intermediate metabolite of the mitochondrial tricarboxylic acid (TCA) cycle, which stabilizes hypoxia-inducible factor-1α (HIF-1α) protein. The increase in HIF-1α further transactivated key glycolytic genes to persistently maintain glycolytic flux in MSCs. Taken together, our findings reveal a novel immunoregulatory mechanism of MSCs involving an NAD^+ metabolism-mediated feedback loop and suggest that augmenting NAMPT activity may increase the therapeutic efficacy of MSCs in the clinical treatment of inflammatory diseases.

MATERIALS AND METHODS

Animals

C57BL/6 J mice were obtained from Charles River Experimental Animal Technology Co., Ltd. (Beijing, China) and maintained in a specific pathogen-free barrier facility of the Laboratory Animal Center of Soochow University. The mice used for tissue harvesting or experimental procedures were males aged between 8 and 10 weeks. These mice were housed in ventilated cages at 21 °C to 23 °C with a 12 h light-dark cycle. The relative humidity in the animal facility was between 40 and 60%. Irradiated food purchased from Jiangsu Xie Tong Pharmaceutical Bioengineering Co., Ltd. (Nanjing, China) and sterile water were provided *ad libitum*. All animal experimental procedures were approved by the Institutional Animal Care and Use Committee of Soochow University (SUDA20210916A07).

MSC isolation and culture

MSCs were isolated and cultured as previously described [25, 26]. Briefly, bone marrow was harvested from the tibias and femurs of C57BL/6 J mice. The cells were cultured in DMEM supplemented with 10% fetal bovine serum (FBS), 2 mM glutamine, 100 U/ml penicillin, and 100 μg/ml streptomycin (all from Invitrogen, Carlsbad, CA). Nonadherent cells were removed after 24 h, and adherent cells were retained. The medium was changed every 3 days. To obtain MSC clones, confluent cells were harvested and seeded into 96-well plates by limited dilution. Individual clones were then chosen and expanded. These MSCs were capable of differentiating into adipocytes and osteocytes under the appropriate differentiation conditions. All details regarding the characterization of cultured MSCs are shown in Fig. S1 of the Supporting Information.

Apoptosis analysis

MSCs were stained with Annexin V and 7-AAD, incubated for 15 min at room temperature (25 °C) in the dark and subsequently analyzed by flow cytometry.

Quantitative real-time polymerase chain reaction

Total RNA was extracted from each sample using TRIzol reagent (Invitrogen) and reverse-transcribed using a QuantiTect Reverse Transcription Kit (Qiagen, Germany) according to the manufacturer's instructions. Gene expression was measured by a QuantStudio 6 Flex System using SYBR Green Master Mix (Applied Biosystems, Foster City, CA). The total amount of mRNA was normalized to endogenous *β-actin* mRNA. The primers for the target genes were designed and are listed in Supplementary Table 1 of the supporting information.

RNA sequencing

Total RNA was extracted from each sample using TRIzol reagent, quantified and purified with a Bioanalyzer 2100 and RNA 6000 Nano LabChip Kit (Agilent, CA) according to the manufacturer's instructions. The RNA libraries were prepared and sequenced on an Illumina Novaseq™ 6000 platform by LC Bio Technology Co., Ltd. (Hangzhou, China). Data analysis and visualization were performed using R (https://www.r-project.org/) and the OmicStudio platform of LC Bio Technology Co., Ltd. (https://www.omicstudio.cn/tool). Specifically, log processing was performed on all data obtained by RNA-seq. Log pretreatment refers to adding a value to the data before log processing, which is applicable when the distribution range of the data crosses orders of magnitude. In this case, log processing can enhance the visualization effect of the heatmap without changing the linear relationship of the data. Then, after log pretreatment these data were processed by centralization, which refers to the value of a gene minus its mean across all samples.

Western blotting

Cells were washed twice with ice-cold PBS, harvested and lysed in RIPA buffer (Beyotime, Shanghai, China) containing a cocktail of protease inhibitors (Roche, Nutley, NJ) and PMSF (Beyotime) for 30 min on ice. The lysates were collected by centrifugation at 12,000 × *g* for 20 min and heated in sodium dodecyl sulfate sample buffer at 95 °C for 10 min. The protein concentration of the supernatant was determined by BCA protein assays (Bio-Rad, Hercules, CA). The protein samples were separated on polyacrylamide gels, transferred onto polyvinylidene fluoride membranes (Millipore, Temecular, CA) and incubated for 1 h in 5% nonfat dry milk dissolved in TBST (150 mM NaCl, 50 mM Tris-HCl, 0.05% Tween 20, pH 7.5) at room temperature. The membranes were incubated with primary antibodies overnight at 4 °C, extensively washed in TBST, incubated with horseradish peroxidase-conjugated secondary antibodies for 2 h at room temperature, and washed again with TBST. The membranes were developed with chemiluminescent detection (Millipore) according to the instructions provided by the manufacturer.

NAMPT knockdown

To achieve NAMPT knockdown, MSCs were transfected with NAMPT-targeting short hairpin RNA (shRNA) carried by a lentiviral vector (PGLV3/H1/GFP/Puro, GenePharma, Shanghai, China) and incubated with polybrene (5 μg/mL, GenePharma) for 12 h. The shRNA target sequence for Nampt was 5′-GGTTACAGAGGAGTCTCTTCG-3′. The scrambled shRNA target sequence was 5′-TTCTCCGAACGTGTCACGT-3′. Puromycin (5 μg/mL, from Gibco, San Francisco, CA) was added to the culture medium to screen successfully transfected cells.

Metabolic assays

Intracellular NAD^+ levels were determined using an NAD^+/NADH Quantitation Colorimetric Kit (Beyotime) according to the manufacturer's instructions. Briefly, 10^6 cells were lysed in 200 μL NAD^+/NADH extraction buffer and centrifuged at 12,000 × *g* for 10 min. Then, 20 μL of the supernatant was directly transferred to a 96-well plate for NAD_{total} (NAD^+ and NADH) measurement, and the residues were heated in a water bath at 60 °C for 30 min for NADH detection. Next, 90 μL of alcohol dehydrogenase working solution was gently added to each well and incubated at 37 °C for 10 min. Subsequently, 10 μL of NADH developer was added and incubated at 37 °C for 30 min. The optical density at 450 nm was measured using a multiwell spectrophotometer. The NAD^+ level in each sample was calculated based on a standard curve drawn with the NADH standards included in the kit.

NO was measured using a modified Griess reagent (Sigma–Aldrich, St. Louis, MO). Briefly, all NO was converted into NO2 by nitrate reductase, and total NO2 was detected by the Griess reaction [27].

Real-time ECAR measurements were made with an Agilent Seahorse XF-24 Extracellular Flux Analyzer. MSCs were plated on 24-well Seahorse XF cell culture microplates and subjected to different experimental processes prior to performing the assay. Seahorse XF base medium was supplemented with 1 mM glutamine, adjusted to pH 7.4 with 0.1 N NaOH and filtered through a 0.22 μm filter. The ECAR was measured under basal conditions and after the addition of the following compounds: 10 mM

glucose, 1 μM oligomycin, and 50 mM 2-DG, which were added to ports A, B, and C of the analyzer, respectively. Subsequently, each solution was added at the indicated time points. The results were collected with Agilent Wave software.

Glucose and lactate in cell culture supernatants were measured with a glucose assay kit and lactate assay kit, respectively (Abcam, New Territories, Hong Kong). Gas chromatography–mass spectrometry (GC–MS)-based targeted metabolomics was performed on MSCs by Applied Protein Technology Co., Ltd. (Shanghai, China) to analyze intracellular glycolytic and TCA cycle intermediates. ATP abundance was measured using an ATP assay kit (Beyotime). Briefly, 10^5 cells were lysed in 200 μL ATP extraction buffer and centrifuged at 12,000 × *g* for 5 min. Then, 20 μL of the supernatant was directly transferred to a white 96-well plate containing 100 μL of ATP detection working solution. Subsequently, the samples were measured using a luminometer.

Succinate abundance was measured using a succinate colorimetric assay kit (Abcam, New Territories, Hong Kong). Briefly, 10^5 cells were lysed in 100 μL succinate assay buffer and centrifuged at 12,000 × *g* for 10 min. Then, 50 μL of the supernatant was directly transferred to a white 96-well plate containing 50 μL of the reaction mix. The plate was incubated at 37 °C for 30 min. Subsequently, the absorbance of the samples was measured at 450 nm using a luminometer.

Splenocyte proliferation assay

The proliferation of splenocytes was detected using CFSE staining and flow cytometry [10]. Briefly, freshly isolated splenocytes in 1 ml of PBS containing 0.1% bovine serum albumin were stained with 5 μM CFSE dye for 10 min in a 37 °C water bath with mixing every 2 min. The reaction was stopped by adding 1 ml of cold FBS. After 5 min, the cells were washed with 5% FBS in PBS. The cells were activated with anti-CD3 (clone: 145-2c-11) and cocultured with MSCs. After 72 h, the cells were collected, and the remaining cell-associated CFSE fluorescence was analyzed by flow cytometry.

Preparation of bone marrow-derived macrophages

To obtain bone marrow-derived macrophages, bone marrow was isolated from the femurs and tibias of C57BL/6 J mice and cultured in DMEM/F12 medium supplemented with 10% FBS and 20% L929 conditioned medium for 7 days. The adherent cells were treated with MSC supernatants for 48 h or subsequently activated with 100 ng/mL LPS (Sigma–Aldrich) for 24 h. MSCs were stimulated with IFN-γ and TNF-α (10 ng/ml each) for 24 h in the presence or absence of 50 nM FK866, washed three times with PBS and subsequently cultured with DMEM for another 24 h before the supernatants were harvested. The MSC supernatant samples were used for the subsequent treatment of mature bone marrow-derived macrophages.

Generation and analysis of the murine acute liver injury model

Male C57BL/6 J mice were intravenously injected with 15 mg/kg ConA (Sigma–Aldrich) in PBS to induce acute liver injury. Bone marrow-derived MSCs (1×10^6) were pretreated with IFN-γ (10 ng/ml) and TNF-α (10 ng/ml) for 12 h and then intravenously administered to mice that had been treated with ConA for 30 min. The mice were euthanized, and serum and liver samples were collected after 12 h. Serum ALT and AST activity were determined by an ALT detection kit and an ALT detection kit, respectively (Nanjing Jiancheng Bioengineering Institute, Nanjing, China). Serum IFN-γ and IL-12 levels were determined by a mouse IFN-γ ELISA kit and a mouse IL-12 ELISA kit (Beyotime), respectively.

Generation and analysis of the murine colitis model

Male C57BL/6 J mice were fed drinking water containing 4% DSS (MP Biomedicals, Santa Ana, CA) *ad libitum* for 7 days to induce colitis. Bone marrow-derived MSCs (1×10^6 or 1×10^5) were intravenously administered to IBD mice on Day 2 after the beginning of DSS treatment. Control mice received normal drinking water. The body weight of each mouse was monitored daily during IBD induction. All experimental mice were euthanized after 7 days of DSS treatment, and colon samples were collected for further processing. Serum IL-6 levels were determined by a mouse IL-6 ELISA kit (Beyotime).

The disease activity index was evaluated after 7 days of DSS treatment by scoring body weight loss (grades, 0–4: 0, none; 1, <10% loss of the initial body weight; 2, 10–15% loss of the initial body weight; 3, 15–20% loss of the initial body weight; and 4, >20% loss of the initial body weight), stool consistency (grades, 0–2: 0, none; 1, mild diarrhea; and 2, moderate to severe diarrhea), rectal bleeding (grades, 0–2: 0, none; 1, mild bleeding; and 2, moderate to severe bleeding), and general activity (grades, 0–2: 0, normal; 1, mildly depressed; and 2, moderately to severely depressed) [28].

H&E staining and histological analysis

Liver and colon tissue samples were fixed in 4% paraformaldehyde for 3 days and sequentially dehydrated with 75% ethanol (overnight), 85% ethanol (1 h), 95% ethanol (1 h), and 100% ethanol (1 h). The samples were treated with xylene twice for 20 min each before being embedded in paraffin. Finally, the samples were cut into 3-μm sections.

Histological analysis was performed using standard hematoxylin and eosin (H&E) staining. The severity of IBD symptoms was evaluated by scoring the extent of bowel wall thickening (grades 0–3: 0, none; 1, mucosa; 2, mucosa and submucosa; and 3, transmural), crypt damage (grades 0–3: 0, none; 1, loss of goblet cells; 2, only the surface epithelium was intact; and 3, loss of the entire crypt and epithelium), and the infiltration of inflammatory cells (grades 0-2: 0, none; 1, mild to moderate; and 2, severe) in H&E-stained colon sections [28].

Isolation of tissue inflammatory cells and flow cytometric analysis

The colon samples were excised, any visible fat was removed, and the samples were rinsed in PBS. The samples were then cut into 1 cm pieces and immersed in warm HBSS containing 5% FBS, 2 mM DTT, and 5 mM EDTA at 37 °C for 20 min on a shaker. The tissue samples were then digested in DMEM containing 10% FBS, collagenase I (1 mg/mL) and dispase (11 U/ml) at 37 °C for 1 h on a shaker. The digested colon tissues were then passed through a 70-μm cell strainer to generate a single cell suspension for 80%/40% Percoll separation. Finally, the collected cells were stained with antibodies specific for CD45, CD11b and F4/80. Flow cytometry data were analyzed using FlowJo [28].

Statistical analysis

All data are represented as the mean and standard error of the mean (mean ± SEM) as specified in the figure legends. Statistical comparisons were made using GraphPad Prism software (Version 8.0, GraphPad Prism Software Inc., San Diego, CA). The number in each treatment group is indicated as "*n*" in the figure legends. For two-group comparisons, a two-tailed unpaired *t* test was performed. For multiple group comparisons, one-way analysis of variance was performed. *P* values are shown in the corresponding figures. Notably, *P* values less than 0.05 were considered statistically significant.

RESULTS

The NAD^+ salvage pathway is upregulated in MSCs stimulated by inflammatory cytokines

NAD^+ deficiency is now being recognized as a major cause of increased metabolic dysfunction and altered disease susceptibility in inflammatory disorders and aging [16, 29–31]. NAD^+ homeostasis is frequently disrupted in activated immune cells, in which accelerated NAD^+ consumption and defective NAD^+ biosynthesis collectively deplete intracellular NAD^+ stores [32–36]. Recent studies have shown that MSCs stimulated by inflammatory cytokines are metabolically wired for aerobic glycolysis, which directly controls their immunoregulatory effects [37–39]. NAD^+, which is a hydrogen carrier, regulates multiple catabolic processes, including glycolysis, the TCA cycle and β-oxidation of fatty acids. Therefore, we hypothesized that NAD^+ equilibrium was necessary for the immunoregulatory capacity of primed MSCs. To explore this hypothesis, we first measured NAD^+ levels over a 24-hour period in MSCs after stimulation with IFN-γ and TNF-α. Compared to that in resting MSCs, NAD^+ abundance gradually decreased in inflammatory cytokine-primed MSCs (Fig. 1A). The decrease in NAD^+ was accompanied by increased expression of the key NAD^+ salvage pathway enzymes NMN adenylyl transferase 2 (NMNAT2) and NAMPT, whereas expression of enzymes in the Preiss-Handler pathway for NAD^+ synthesis from nicotinic acid and the de novo biosynthetic pathway from tryptophan remained unchanged,

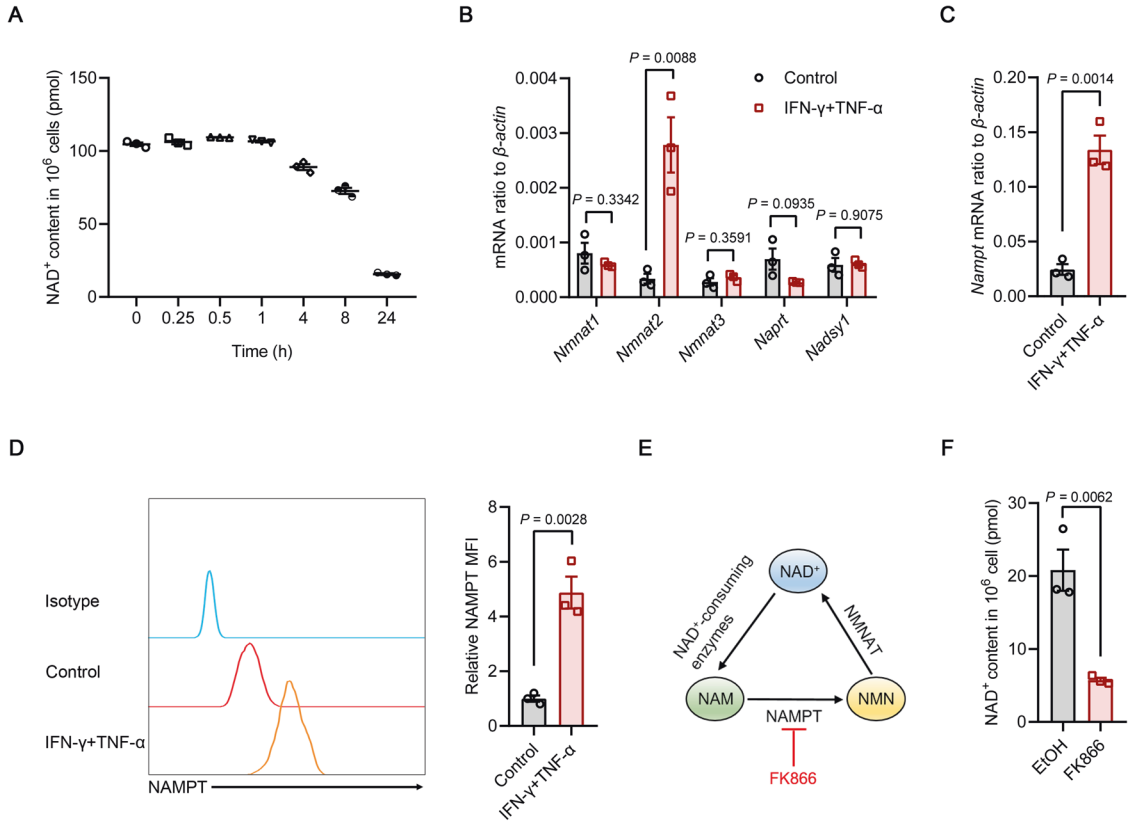

Fig. 1 The NAD$^+$ salvage pathway is upregulated in inflammatory cytokine-primed MSCs. **A** NAD$^+$ levels in MSCs stimulated with IFN-γ and TNF-α (10 ng/ml each) over time ($n = 3$). **B** The expression of NAD$^+$-related biosynthetic enzymes in MSCs stimulated with IFN-γ and TNF-α (10 ng/ml each) for 24 h was assayed by quantitative real-time polymerase chain reaction (qRT–PCR) ($n = 3$). **C** The expression of *Nampt* mRNA in MSCs stimulated with IFN-γ and TNF-α (10 ng/ml each) for 24 h was assayed by qRT–PCR ($n = 3$). **D** Flow cytometric analysis of NAMPT protein expression in MSCs stimulated with IFN-γ and TNF-α (10 ng/ml each) for 24 h ($n = 3$). **E** Schematic representation of the NAD$^+$ salvage pathway. **F** NAD$^+$ levels in MSCs stimulated with IFN-γ and TNF-α (10 ng/ml each) for 24 h in the presence or absence of 50 nM FK866 ($n = 3$). MFI, mean fluorescence intensity. Values are presented as the mean ± SEM. Statistical analysis was performed by two-tailed unpaired *t* test

suggesting that the NAD$^+$ salvage pathway contributes to the maintenance of NAD$^+$ levels in IFN-γ/TNF-α-stimulated MSCs (Fig. 1B–D). Indeed, when MSCs were treated with FK866, which potently and specifically inhibits NAMPT enzymatic activity in a competitive manner with minimum toxicity and no impact on NAMPT expression (Fig. 1E and Supplementary Fig. 2A–C) [40], the NAD$^+$ pool was further exhausted in MSCs in response to inflammatory priming (Fig. 1F). Collectively, these results suggested that inflammatory cytokine-primed MSCs rely on NAMPT to maintain intracellular NAD$^+$ levels.

NAMPT function is required for the expression of chemokines and immunomodulatory genes in inflammatory cytokine-primed MSCs

We next investigated the role of NAMPT in the immunomodulatory function of inflammatory cytokine-primed MSCs. RNA sequencing (RNA-seq) was performed on bone marrow-derived MSCs treated with IFN-γ and TNF-α for 24 h in the presence or absence of FK866. The results indicated that FK866 did not affect stemness characteristics or induce cellular senescence in inflammatory cytokine-primed MSCs (Supplementary Fig. 3). However, NAMPT inhibition decreased the expression of genes associated with chemotaxis and immune responses that are normally induced in response to inflammatory cues, as determined using gene set enrichment analysis (GSEA) (Fig. 2A). Specifically, FK866 treatment had broad negative effects on the expression of genes encoding various CC-chemokine ligand (CCL) members, CXC-chemokine ligand (CXCL) members and anti-inflammatory mediators (Fig. 2B and Supplementary Fig. 4A). Given that MSC-mediated immunomodulation involves CCR5 ligands and CXCR3 ligands, including CCL5, CXCL9 and CXCL11, as well as multiple anti-inflammatory factors, such as heme oxygenase 1 (HO1), cyclooxygenase 2 (COX2) and iNOS [2, 4, 5], we examined the expression of these chemokines and anti-inflammatory genes in primed MSCs after NAMPT inhibition. Consistently, FK866 significantly impaired the production of the chemokines CCL5, CXCL9 and CXCL11 and decreased the expression of the anti-inflammatory factors HO1, COX2 and iNOS (Fig. 2C–G). However, FK866 did not alter the expression levels of these chemokines and anti-inflammatory factors in resting MSCs (Supplementary Fig. 2D–F). In addition, the production of NO, which is cytotoxic to activated T cells, was attenuated in IFN-γ/TNF-α-stimulated MSCs treated with FK866 (Fig. 2H). To further elucidate the importance of NAMPT for inflammatory cytokine-primed MSCs, we used lentivirus-loaded shRNA to reduce NAMPT expression (Supplementary Fig. 5A). Nampt shRNA-treated MSCs, in which NAD$^+$ levels were decreased, expressed fewer chemokines and immunosuppressive factors in response to inflammatory cytokine activation than scrambled shRNA-treated cells (Supplementary Fig. 5B–H).

Given that NMN is the direct downstream metabolite of NAMPT in the NAD$^+$ salvage pathway [41], we reasoned that NMN could rescue the immunosuppressive defects of MSCs due to NAMPT inhibition. Consistent with this idea, supplementation with NMN increased NAD$^+$ levels in IFN-γ/TNF-α-stimulated MSCs treated with FK866, although it failed to fully restore NAD$^+$

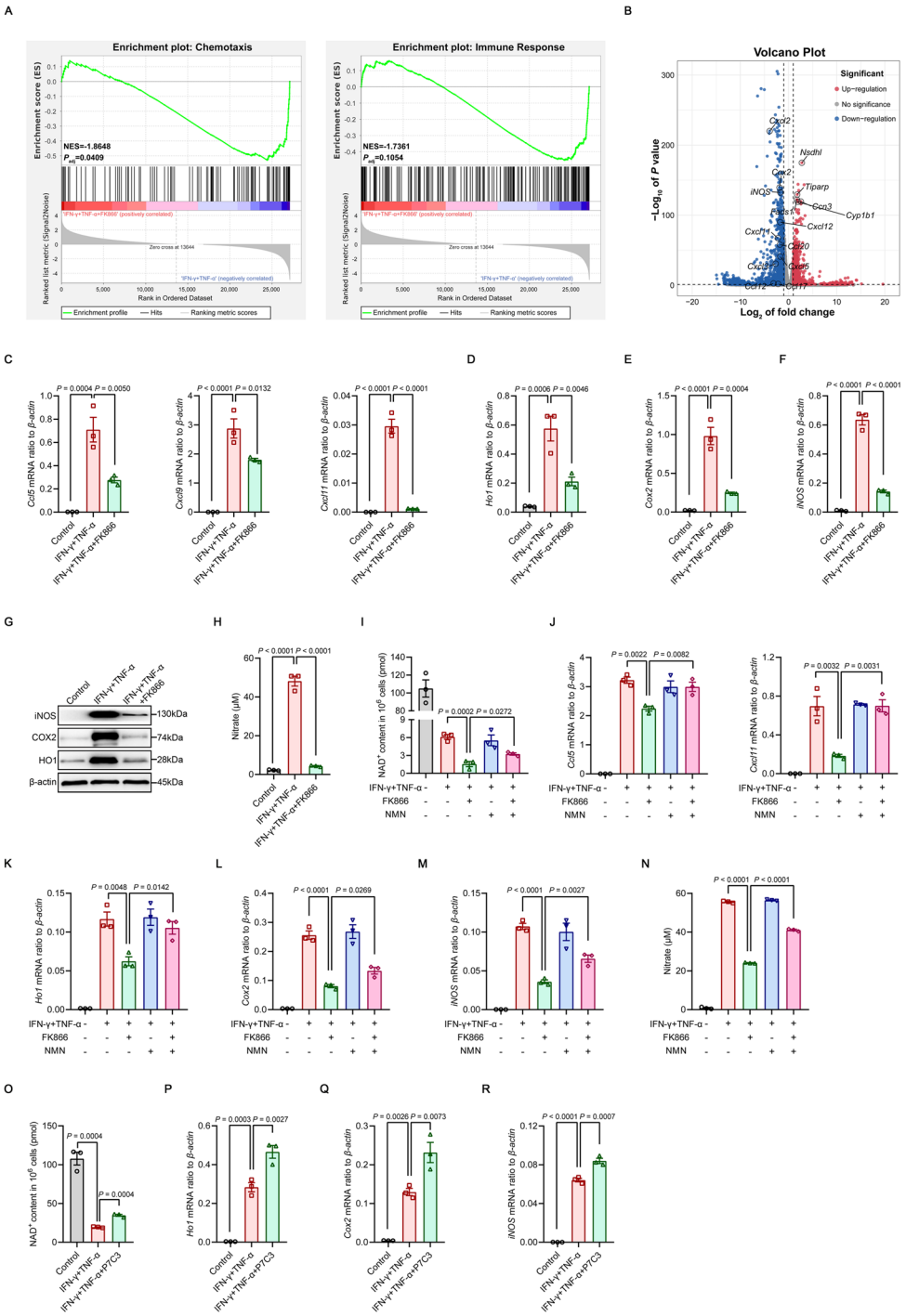

Fig. 2 NAMPT function is required for the expression of chemokines and immunomodulatory genes in inflammatory cytokine-primed MSCs. **A**, **B** RNA-seq was performed on MSCs stimulated with IFN-γ and TNF-α (10 ng/ml each) for 24 h in the presence or absence of 50 nM FK866. The enrichment of chemotaxis and immune response genes was analyzed by GSEA. NES, normalized enrichment score; *P*adj, adjusted *P* value: two-tailed, corrected for multiple comparisons using the Benjamini–Hochberg method (**A**). Volcano plot of differentially expressed chemokine and anti-inflammatory mediator genes (**B**) ($n = 3$). **C**–**F** The expression of chemokines and immunomodulatory genes in MSCs stimulated with IFN-γ and TNF-α (10 ng/ml each) for 24 h in the presence or absence of 50 nM FK866 was assayed by qRT–PCR ($n = 3$). **G** The expression of HO1, COX2, iNOS and β-actin (loading control) in MSCs stimulated with IFN-γ and TNF-α (10 ng/ml each) for 24 h in the presence or absence of 50 nM FK866 were determined by immunoblotting. **H** MSCs were stimulated with IFN-γ and TNF-α (10 ng/ml each) for 24 h in the presence or absence of 50 nM FK866, and the supernatants was assayed for nitrate by a modified Griess reagent ($n = 3$). **I** NAD^+ levels in MSCs stimulated with IFN-γ and TNF-α (10 ng/ml each) with or without 50 nM FK866, 1 mM NMN or both for 24 h ($n = 3$). **J**–**M** The expression of chemokines and immunomodulatory genes in MSCs stimulated with IFN-γ and TNF-α (10 ng/ml each) with or without 50 nM FK866, 1 mM NMN or both for 24 h were determined by qRT–PCR ($n = 3$). **N** MSCs were stimulated with IFN-γ and TNF-α (10 ng/ml each) for 24 h in the presence or absence of 50 nM FK866 and 1 mM NMN, and the supernatants was assayed for nitrate by a modified Griess reagent ($n = 3$). **O** NAD^+ levels in MSCs stimulated with IFN-γ and TNF-α (5 ng/ml each) for 24 h in the presence or absence of 5 μM P7C3 ($n = 3$). **P**–**R** The expression of immunomodulatory genes in MSCs stimulated with IFN-γ and TNF-α (5 ng/ml each) for 24 h in the presence or absence of 5 μM P7C3 was assayed by qRT–PCR ($n = 3$). Values are presented as the mean ± SEM. Statistical analysis was performed by one-way analysis of variance

levels (Fig. 2I). The rescue of metabolic defects by the addition of NMN was accompanied by the reversal of FK866-mediated inhibition of the expression of chemokines and immunomodulatory genes (Fig. 2J–M). More importantly, NMN restored most of the NO production (Fig. 2N). These results collectively suggest that the expression of immunomodulatory genes in inflammatory cytokine-primed MSCs highly relies on a constant NAD^+ supply.

P7C3, an aminopropyl carbazole, increases NAD^+ synthesis from NAM and increases NAD^+ levels by activating NAMPT in the NAD^+ salvage pathway. P7C3 has shown impressive therapeutic efficacy in diseases characterized by NAMPT dysfunction-related NAD^+ decline, including neurodegeneration, diabetes and nonalcoholic fatty liver disease [16, 31, 42, 43]. Consistent with the results from previous reports, increasing NAD^+ levels by enhancing NAMPT activity using P7C3 significantly increased the expression of various anti-inflammatory genes (Fig. 2O–R), although it failed to further enhance the levels of chemokines (Supplementary Fig. 6A). However, P7C3 did not enhance the expression levels of immunosuppressive factors in resting MSCs (Supplementary Fig. 6B), suggesting that inflammatory licensing is a prerequisite for inducing the expression of immunomodulatory genes in MSCs [4]. Taken together, these data suggest that the NAD^+ salvage pathway is required for the expression of chemokines and immunomodulatory genes in inflammatory cytokine-primed MSCs.

NAMPT is essential for the immunomodulatory effects of MSCs on T cells and macrophages

To further explore whether NAMPT dysfunction could weaken the immunoregulatory effects of MSCs on immune cells, we cocultured FK866-pretreated MSCs with activated splenocytes at a 1:20 ratio (MSC-to-splenocyte) for 3 days. The proliferation of splenocytes was measured by the carboxyfluorescein diacetate succinimidyl ester (CFSE) dilution assay. As shown in Fig. 3A, primed MSCs inhibited the proliferation of splenocytes. However, this inhibitory effect of MSCs was significantly compromised after FK866 treatment. In addition, we treated bone marrow-derived macrophages with different MSC supernatants. FK866-treated MSC supernatant was not effective in increasing the expression of the anti-inflammatory genes *arginase 1* (*Arg-1*), *chitinase-like 3* (*Chil3*), *Cd206* and *transforming growth factor β* (*Tgf-β*) in mature macrophages (Fig. 3B). Furthermore, the ability of MSCs to reduce the proinflammatory genes *Il-6*, *Il-12* and *Tnf-α* in inflammatory macrophages was greatly weakened after LPS challenge (Fig. 3C). Consistently, NAMPT knockdown using shRNA interfered with MSC-mediated inhibition of splenocyte proliferation (Fig. 3D). The MSC-induced expression of anti-inflammatory genes in mature macrophages was blocked by *Nampt*-shRNA (Fig. 3E). Importantly, the decrease in the expression of proinflammatory genes was abolished in LPS-stimulated macrophages treated with *Nampt*-shRNA MSC supernatant (Fig. 3F).

Next, we investigated whether NMN supplementation in MSCs with NAMPT loss of function could restore the immunomodulatory effects of MSCs on T cells and macrophages. Consistent with the reversal of FK866-mediated inhibition of the expression of immunoregulatory factors, NMN treatment restored the suppressive effects of FK866-treated MSCs on the activation and proliferation of splenocytes (Supplementary Fig. 7A). Additionally, the addition of NMN rescued the defects in anti-inflammatory macrophage polarization associated with FK866-treated MSC supernatant, which was characterized by increased expression of the anti-inflammatory genes *Arg-1*, *Chil3*, *Cd206* and *Tgf-β* and decreased production of the proinflammatory cytokines *Il-6*, *Il-12* and *Tnf-α* in bone marrow-derived macrophages (Supplementary Fig. 7B, C). Taken together, these data suggest that NAMPT function is essential for the immunomodulatory effects of MSCs on T cells and macrophages.

MSCs alleviate inflammatory diseases in a NAMPT-dependent manner

We next used the dextran sulfate sodium (DSS)-induced IBD mouse model to investigate the role of NAMPT in the immunomodulatory function of MSCs in vivo (Fig. 4A). DSS-induced IBD is a well-established model of intestinal epithelial injury induced by acute innate immune responses, and inflammatory macrophages are the major effector cells [44]. Moreover, the appearance of colitis in severe combined immunodeficiency (SCID) and $Rag^{-/-}$ mice indicates that acute DSS-induced colitis can arise in the absence of adaptive immune cells [45, 46]. As expected, a single intravenous injection of scrambled-shRNA MSCs significantly improved clinical parameters such as body weight and disease activity index compared to those in colitic mice treated with PBS (Fig. 4B, C). Scrambled-shRNA MSC-treated IBD mice also had a significantly lower reduction in colon length (Fig. 4D). Moreover, scrambled-shRNA MSCs reduced the extent of bowel wall thickening and crypt damage in colons, as shown by histological examination (Fig. 4E). More importantly, scrambled-shRNA MSCs decreased serum levels of IL-6 (Fig. 4F), which is an important indicator of colitis progression [47]. Detailed analysis of immune cells in the injured colon showed that the infiltration of inflammatory cells was dramatically decreased in mice that were administered scrambled-shRNA MSCs (Fig. 4G). In contrast, *Nampt*-shRNA MSCs were not effective in ameliorating clinical parameters, increasing colon length or reducing serum IL-6 in mice with colitis (Fig. 4B–F). In addition, *Nampt*-shRNA MSCs failed to reduce the numbers of infiltrated inflammatory cells in the colon tissues of DSS-treated mice (Fig. 4G).

We established a concanavalin A (ConA)-induced acute liver injury model to further validate the therapeutic efficacy of MSCs in inflammatory diseases (Supplementary Fig. 8A). ConA-induced liver injury is a well-recognized in vivo model of hepatocyte apoptosis induced by acute adaptive immune responses, in which excessive T lymphocyte proliferation is the major contributor [48]. Scrambled-shRNA MSCs significantly alleviated liver damage, leading to dramatic reductions in serum alanine transaminase (ALT) and aspartate transaminase (AST) levels, proinflammatory mediators, and centrilobular necrosis. However, these beneficial effects were not observed in *Nampt*-shRNA MSC-treated mice (Supplementary Fig. 8B–D). These results demonstrated that NAMPT was required for the therapeutic efficacy of MSCs in inflammatory diseases.

We next attempted to determine whether increasing NAMPT activity could enhance the therapeutic potential of infused MSCs in inflammatory diseases. In this context, a single intravenous injection of MSCs at a lower dose was not effective in ameliorating IBD and acute liver injury. However, the same dose of P7C3-pretreated MSCs exerted significant therapeutic effects on mice with colitis and acute liver injury (Fig. 4H-N and Supplementary Fig. 8E–H). Taken together, these data suggest that the therapeutic efficacy of MSCs in inflammatory diseases depends on NAMPT.

NAMPT sustains inflammatory cytokine-induced glycolysis in MSCs

Recent studies have shown that inflammatory factors trigger metabolic skewing toward aerobic glycolysis in MSCs, which directly determines their immunoregulatory effects [37–39]. Moreover, cellular NAD^+ availability determines whether cells engage in aerobic glycolysis [49]. To further characterize the role of NAMPT-dependent NAD^+ salvage in glycolysis after inflammatory priming, we analyzed the RNA-seq data of IFN-γ/TNF-α-stimulated MSCs treated with FK866. GSEA signatures showed that the genes that were enriched for glycolysis were downregulated in inflammatory cytokine-primed MSCs treated with the NAMPT inhibitor (Fig. 5A). Specifically, we found that FK866 significantly decreased the expression of key glycolytic genes, including

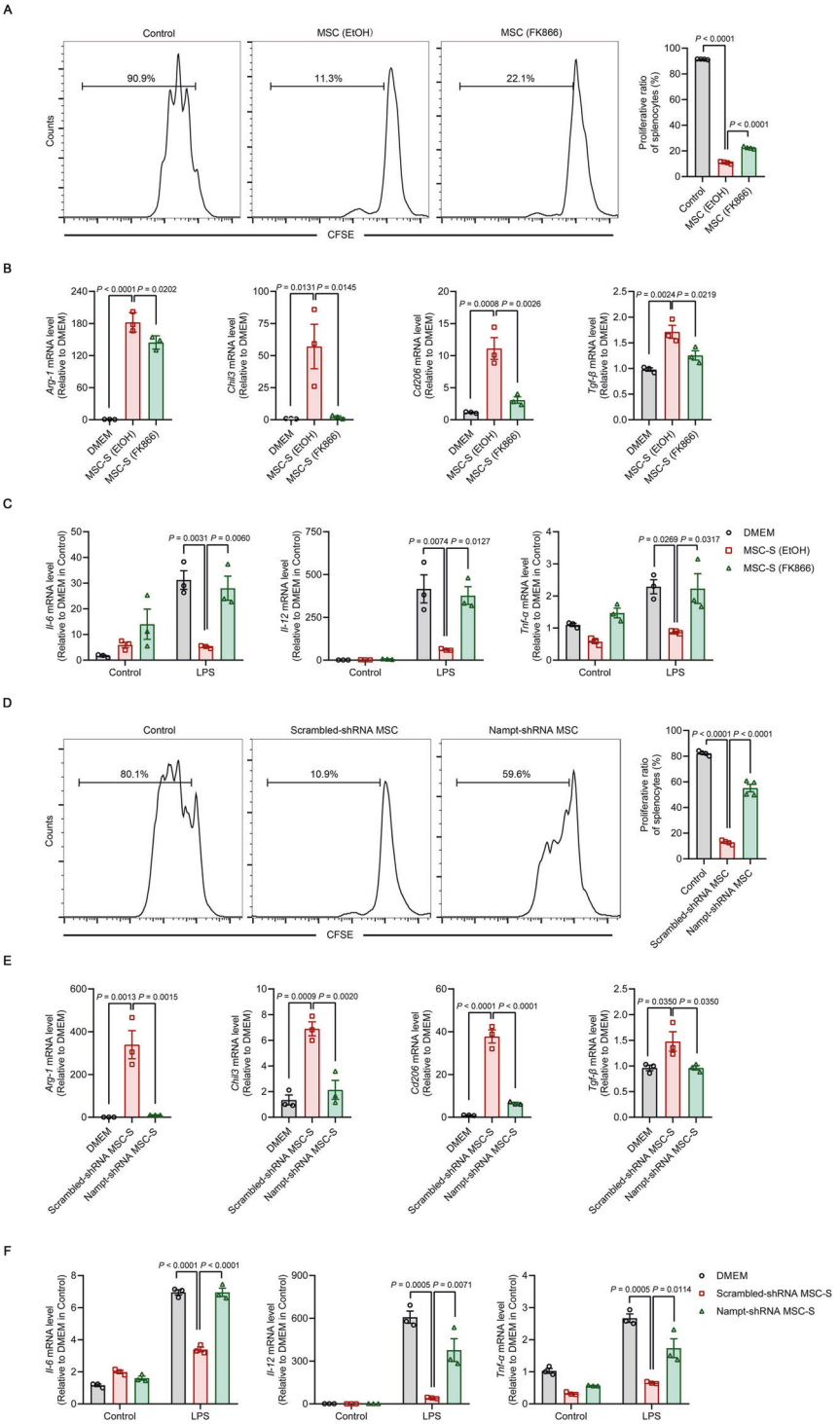

Fig. 3 NAMPT is required for the immunomodulatory effects of MSCs on T cells and macrophages. **A** Splenocytes were stained with CFSE and cocultured with EtOH-pretreated MSCs or FK866-pretreated MSCs (2.5×10^4 cells per well in 48-well plates) at a ratio of 1:20 (MSC:splenocyte) for 72 h in the presence of anti-CD3 (1 μg/ml). The reduction in the CFSE fluorescence intensity in splenocytes was detected by flow cytometry ($n = 4$). **B** Bone marrow-derived macrophages (BMDMs) were treated with different MSC supernatants (MSC-S) for 48 h. The expression of anti-inflammatory genes *Arg-1*, *Chil3*, *Cd206* and *Tgf-β* in mature BMDMs was determined by qRT–PCR ($n = 3$). **C** BMDMs were treated with different MSC-S for 48 h and subsequently treated with LPS (100 ng/mL) for 24 h. The expression of the proinflammatory genes *Il-6*, *Il-12* and *Tnf-α* in inflammatory macrophages was determined by qRT–PCR ($n = 3$). **D** Splenocytes were stained with CFSE and cocultured with Scrambled-shRNA or *Nampt*-shRNA MSCs (2.5×10^4 cells per well in 48-well plates) at a ratio of 1: 20 (MSC:splenocyte) for 72 h in the presence of anti-CD3 (1 μg/ml). The reduction in the CFSE fluorescence intensity in splenocytes was detected by flow cytometry ($n = 4$). **E** BMDMs were treated with different MSC-S for 48 h. The expression of the anti-inflammatory genes *Arg-1*, *Chil3*, *Cd206* and *Tgf-β* in mature BMDMs was determined by qRT–PCR ($n = 3$). **F** BMDMs were treated with different MSC-S for 48 h and subsequently treated with LPS (100 ng/mL) for 24 h. The expression of the proinflammatory genes *Il-6*, *Il-12* and *Tnf-α* in inflammatory macrophages was determined by qRT–PCR ($n = 3$). Values are presented as the mean ± SEM. Statistical analysis was performed by one-way analysis of variance

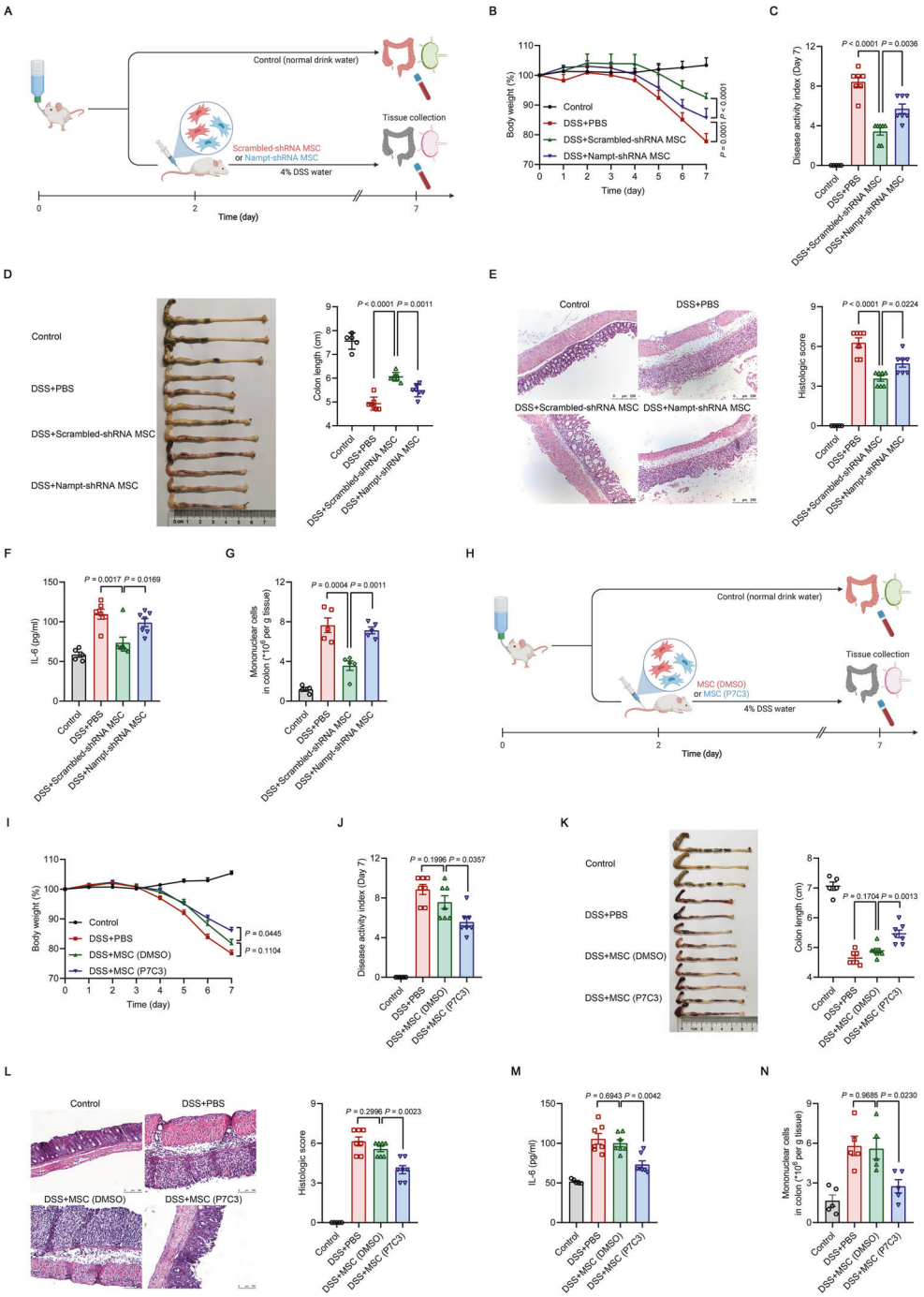

Fig. 4 The beneficial effects of MSCs on inflammatory bowel disease (IBD) require NAMPT. **A** Treatment of DSS-induced IBD by Scrambled-shRNA or *Nampt*-shRNA MSCs (1×10^6) administered intravenously to mice on Day 2 after the beginning of DSS treatment. Mice in the control group received normal drinking water. On Day 7, the mice were euthanized, and the colons were excised. **B**–**D** Body weight, disease activity index and colon length of IBD mice treated with Scrambled-shRNA or *Nampt*-shRNA MSCs. **E** Representative H&E-stained colon sections and histological scores of IBD mice treated with scrambled-shRNA or *Nampt*-shRNA MSCs. Scale bars, 250 μm. **F** Interleukin-6 (IL-6) levels in the serum of IBD mice treated with Scrambled-shRNA or *Nampt*-shRNA MSCs were assayed by enzyme-linked immunosorbent assay (ELISA) (Control: $n = 5$, DSS + PBS: $n = 7$, DSS+Scrambled-shRNA MSC: $n = 7$, DSS+*Nampt*-shRNA MSC: $n = 7$). **G** Mononuclear cell counts in the colon lamina propria of IBD mice treated with Scrambled-shRNA or *Nampt*-shRNA MSCs, as determined by flow cytometry (Control: $n = 4$, DSS + PBS: $n = 5$, DSS+Scrambled-shRNA MSC: $n = 5$, DSS+*Nampt*-shRNA MSC: $n = 5$). **H** Treatment of DSS-induced IBD by DMSO-pretreated MSCs or P7C3-pretreated MSCs (1×10^5) administered intravenously to mice on Day 2 after the beginning of DSS treatment. Mice in the control group received normal drinking water. On Day 7, the mice were euthanized, and the colons were excised. **I**–**K** Body weight, disease activity index and colon length of IBD mice administered DMSO-pretreated MSCs or P7C3-pretreated MSCs. **L** Representative H&E-stained colon sections and histological scores of IBD mice administered DMSO-pretreated MSCs or P7C3-pretreated MSCs. Scale bars, 100 μm. **M** IL-6 levels in the serum of IBD mice administered DMSO-pretreated MSCs or P7C3-pretreated MSCs were assayed by ELISA (Control: $n = 5$, DSS + PBS: $n = 7$, DSS + MSC (DMSO): $n = 7$, DSS + MSC (P7C3): $n = 7$). **N** Mononuclear cell counts in the colon lamina propria of IBD mice administered DMSO-pretreated MSCs or P7C3-pretreated MSCs, as determined by flow cytometry (Control: $n = 5$, DSS + PBS: $n = 5$, DSS + MSC (DMSO): $n = 5$, DSS + MSC (P7C3): $n = 5$). Values are presented as the mean ± SEM. Statistical analysis was performed by one-way analysis of variance

glucose transporter 1 (*Glut1*), *hexokinase 2* (*Hk2*), *phosphofructokinase* (*Pfkl*), *aldolase-fructose-bisphosphate A* (*Aldoa*), *glyceraldehyde-3-phosphate dehydrogenase* (*Gapdh*), *phosphoglycerate mutase 1* (*Pgam1*), *enolase 1* (*Eno1*), *pyruvate kinase M1/2* (*Pkm*) and *lactate dehydrogenase A* (*Ldha*) (Fig. 5B, C). The protein levels of GLUT1 (the glucose transporter) and HK2 (the pacemaker molecule for glycolysis) were downregulated in IFN-γ/TNF-α-primed MSCs in response to NAMPT inhibition (Fig. 5D, E). We measured the extracellular acidification rate (ECAR) to assess glycolytic activity in primed MSCs. Consistently, the robust increase in glycolytic flux typical of inflammatory cytokine-primed MSCs was markedly reduced in the presence of FK866, and the glycolytic rate and capacity were nearly absent (Fig. 5F). Measurements of glycolytic and TCA metabolites revealed significant decreases in many intermediate metabolites and adenosine triphosphate (ATP) production in FK866-treated primed MSCs (Fig. 5G, H).

We next used *Nampt* shRNA-treated MSCs to corroborate the results obtained with FK866. Consistently, the expression of glycolysis-related molecules, including GLUT1 and HK2, was lower than that in MSCs transduced with the scrambled shRNA (Fig. 5I–K). *Nampt* knockdown mirrored glycolysis inhibition observed in response to FK866, as indicated by the decreased glycolytic rate, decreased glucose consumption and lactate accumulation, and reduced intracellular ATP levels (Fig. 5L–N). In addition, we used the hexokinase inhibitor 2-deoxyglucose (2-DG) to specifically block glycolytic processes. The expression of immunoregulatory factors and NO production were dramatically decreased in IFN-γ/TNF-α-stimulated MSCs treated with 2-DG, which mimicked the effects of FK866 (Supplementary Fig. 9). Taken together, these data suggest that NAMPT is important for glycolytic wiring in inflammatory cytokine-primed MSCs.

HIF-1α mediates NAD^+-driven glycolysis in inflammatory cytokine-primed MSCs

To further elucidate the mechanism underlying the reduction in glycolysis caused by NAMPT inhibition in inflammatory cytokine-primed MSCs, we performed Gene Ontology (GO) enrichment analysis, Kyoto Encyclopedia of Genes and Genomes (KEGG) enrichment analysis and GSEA of the RNA-seq data and found that processes related to the cellular response to hypoxia and the HIF-1 signaling pathway were highly enriched and dramatically downregulated in inflammatory cytokine-primed MSCs treated with FK866, suggesting that HIF-1 may be a crucial regulator of NAMPT-dependent glycolysis (Fig. 6A, B and Supplementary Fig. 4B, C). Since the majority of glycolytic genes, including *Glut1*, *Hk2*, *Pfkl*, *Aldoa*, *Eno1*, *Pkm* and *Ldha*, are transactivated by HIF-1α [50], we measured the levels of HIF-1α protein in NAMPT-dysfunctional MSCs in response to inflammatory priming. As expected, HIF-1α levels were greatly increased in MSCs treated with IFN-γ/TNF-α, and this upregulation was abolished by FK866 treatment or NAMPT knockdown (Fig. 6C, D). To determine whether HIF-1α was required for glycolytic activity in MSCs following inflammatory stimulation, we treated IFN-γ/TNF-α-primed MSCs with KC7F2, a selective inhibitor of HIF-1α [51], and observed a decrease in the glycolytic rate, as indicated by decreased levels of numerous glycolytic genes, as well as reduced expression of anti-inflammatory genes (Fig. 6E–I). In contrast, the prolyl hydroxylase (PHD) inhibitor dimethyloxallyl glycine (DMOG), which stabilizes the HIF-1α protein [52], further increased the levels of these glycolytic genes and subsequently increased anti-inflammatory gene expression (Fig. 6E–I). Collectively, these data indicate that HIF-1α drives aerobic glycolysis in inflammatory cytokine-primed MSCs.

The increase in glycolytic activity was accompanied by the upregulation of NAMPT expression in response to enhanced NAD^+ expenditure in inflammatory cytokine-primed MSCs treated with DMOG. Decreased glycolytic flux in response to KC7F2 treatment, on the other hand, spared the reserve of NAD^+ and consequently reduced NAMPT expression, suggesting that NAMPT may sense the fluctuation in NAD^+ levels and increase or decrease its expression accordingly to maintain cellular energy homeostasis (Fig. 6J, K). Next, we determined whether HIF-1α stabilization relied on NAMPT-dependent production of NAD^+. The addition of NMN, the immediate precursor of NAD^+ in the salvage pathway, partially restored HIF-1α protein levels and the subsequent expression of glycolytic genes that were reduced by FK866 (Fig. 6L and Supplementary Fig. 10A). However, HIF-1α inhibition via KC7F2 abrogated the rescue of glycolytic activity and immunomodulatory gene expression by the addition of NMN (Fig. 6M, N and Supplementary Fig. 10B, C). Taken together, these results demonstrate that NAD^+-driven glycolysis in inflammatory cytokine-primed MSCs is mediated by HIF-1α.

The succinate-HIF-1α axis promotes the expression of immunomodulatory effectors in inflammatory cytokine-primed MSCs

Enhanced glycolytic activity is accompanied by increased accumulation of the key TCA cycle intermediate succinate. High levels of succinate are transported from the mitochondria through the dicarboxylic acid transporter to the cytosol, where excess levels impair PHD activity through product inhibition, leading to HIF-1α stabilization and activation [53–55]. As shown in Fig. 5G, NAMPT inhibition decreased succinate levels in primed MSCs. Therefore, we explored whether succinate was responsible for HIF-1α stabilization and sustained the immunomodulatory ability of MSCs. As expected, supplementation with succinate significantly restored HIF-1α protein levels in IFN-γ/TNF-α-stimulated MSCs treated with FK866 (Fig. 7A). However, the impaired production of chemokines and anti-inflammatory factors in the presence of FK866 was only slightly restored by the addition of exogenous succinate, and there was mild rescue of glycolytic defects accompanied by enhanced NAD^+ use (Supplementary Fig. 11A–D). These results indicate that while succinate can stabilize HIF-1α, its effect on increasing glycolysis is limited when the NAD^+ supply is blocked. However, when there was no impairment in NAD^+ supply, succinate supplementation could increase glycolytic activity and consequently increase the expression of chemokines and anti-inflammatory factors in IFN-γ/TNF-α-stimulated MSCs (Supplementary Fig. 11A–C). To further test whether HIF-1α mediates the beneficial effects of succinate, we measured the expression of immunomodulatory genes in inflammatory cytokine-primed MSCs treated with FK866 and succinate in the presence of the HIF-1α inhibitor KC7F2. As expected, HIF-1α inhibition abrogated the effect of the addition of succinate (Supplementary Fig. 11E, F).

Importantly, succinate priming increased the therapeutic efficacy of MSCs in the disease setting. While a single intravenous injection of MSCs at a lower dose was not effective in ameliorating IBD, succinate-pretreated MSCs at the same dose exerted significant therapeutic effects on colitis mice (Fig. 7B–G). We also tested the cell-permeable molecule dimethyl malonate (DMM), which is rapidly hydrolyzed within the cell to generate malonate, a potent competitive inhibitor of succinate oxidation, impairing the oxidation of succinate to fumarate via potent competitive inhibition of succinate dehydrogenase (SDH) and consequently leading to an increase in succinate in the cytosol [56]. DMM increased glycolytic rates and the expression of immunomodulatory genes, which was accompanied by enhanced NAD^+ expenditure (Supplementary Fig. 12). Taken together, these findings indicate that succinate drives HIF-1α-mediated immunomodulation by inflammatory cytokine-primed MSCs.

DISCUSSION

MSCs can orchestrate inflammatory microenvironments and have been widely used to resolve various pathological conditions in

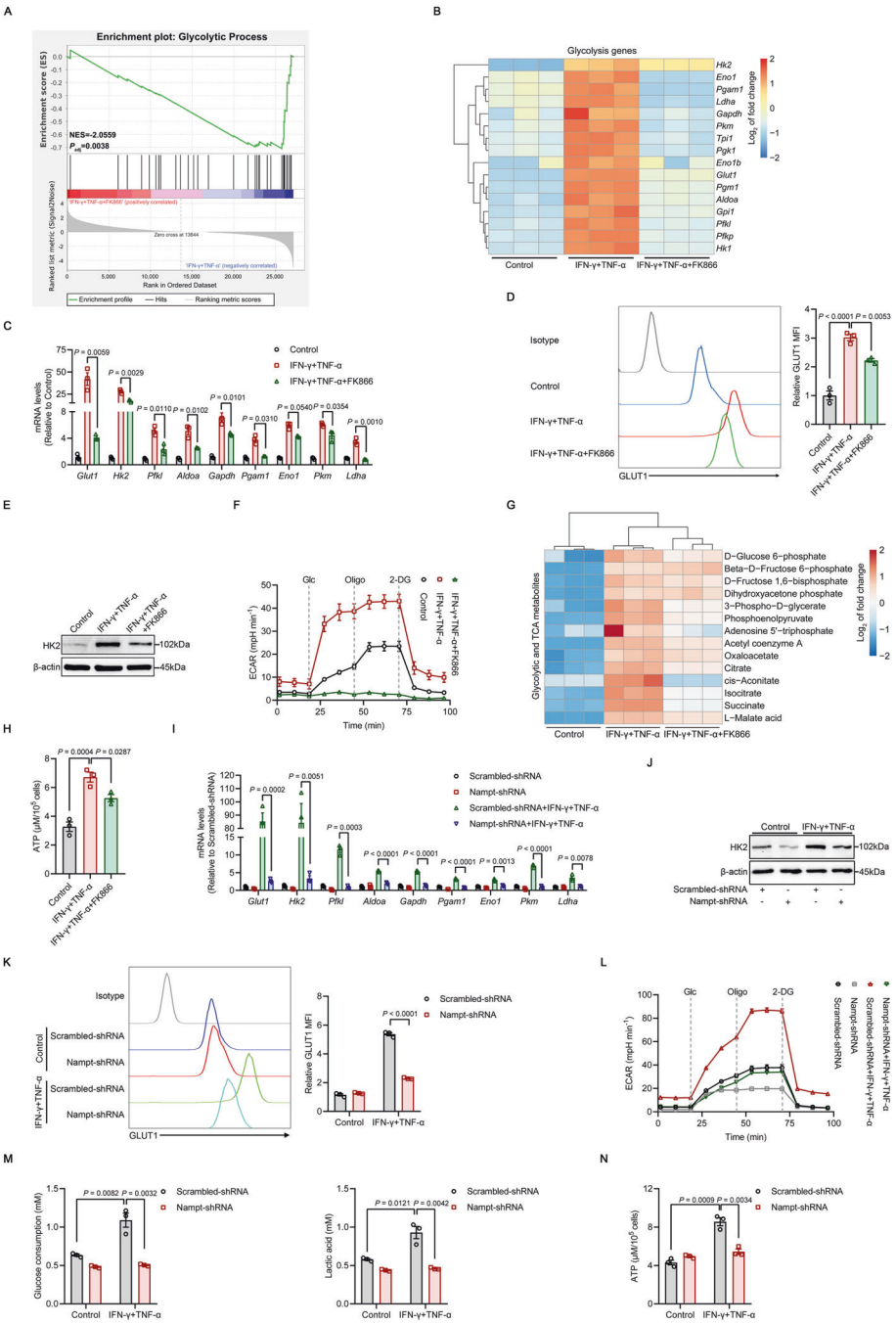

Fig. 5 Primed MSCs require NAMPT to drive glycolysis. **A, B** RNA-seq was performed on MSCs stimulated with IFN-γ and TNF-α (10 ng/ml each) for 24 h in the presence or absence of 50 nM FK866. The enrichment of glycolytic genes process was analyzed by GSEA. NES, normalized enrichment score; *P*adj, adjusted *P* value: two-tailed, corrected for multiple comparisons using the Benjamini–Hochberg method (**A**). Hierarchical clustering of glycolysis-related gene expression (**B**) ($n = 3$). **C** The expression of several glycolytic genes in MSCs stimulated with IFN-γ and TNF-α (10 ng/ml each) for 24 h in the presence or absence of 50 nM FK866 was assayed by qRT–PCR ($n = 3$). **D, E** GLUT1 expression was examined by flow cytometry, and HK2 expression was examined by immunoblotting in MSCs stimulated with IFN-γ and TNF-α (10 ng/ml each) for 24 h in the presence or absence of 50 nM FK866 ($n = 3$). **F** Real-time ECAR changes in MSCs stimulated with IFN-γ and TNF-α (10 ng/ml each) combined with 50 nM FK866 for 24 h using the Seahorse Analyzer ($n = 3$). Glc, glucose; Oligo, oligomycin; 2-DG, 2-deoxyglucose. **G** Hierarchical clustering of targeted metabolomics in MSCs stimulated with IFN-γ and TNF-α (10 ng/ml each) for 24 h in the presence or absence of 50 nM FK866 ($n = 3$). **H** ATP levels in MSCs stimulated with IFN-γ and TNF-α (10 ng/ml each) for 24 h in the presence or absence of 50 nM FK866 ($n = 3$). **I** The expression of several glycolytic genes in MSCs that were transduced with Scrambled-shRNA or *Nampt*-shRNA and stimulated with IFN-γ and TNF-α (10 ng/ml each) for 24 h was assayed by qRT–PCR ($n = 3$). **J, K** GLUT1 expression was examined by flow cytometry, and HK2 expression was examined by immunoblotting in MSCs transduced with Scrambled-shRNA or *Nampt*-shRNA and stimulated with IFN-γ and TNF-α (10 ng/ml each) for 24 h ($n = 3$). **L** Real-time ECAR changes in MSCs transduced with Scrambled-shRNA or *Nampt*-shRNA and stimulated with IFN-γ and TNF-α (10 ng/ml each) using a Seahorse Analyzer ($n = 3$). **M** Analysis of 24-h glucose consumption and lactate production in the supernatant of MSCs transduced with Scrambled-shRNA or *Nampt*-shRNA and stimulated with IFN-γ and TNF-α (10 ng/ml each) ($n = 3$). **N** ATP levels in MSCs transduced with Scrambled-shRNA or *Nampt*-shRNA and stimulated with IFN-γ and TNF-α (10 ng/ml each) for 24 h ($n = 3$). MFI, mean fluorescence intensity. Values are presented as the mean ± SEM. Statistical analysis was performed by one-way analysis of variance

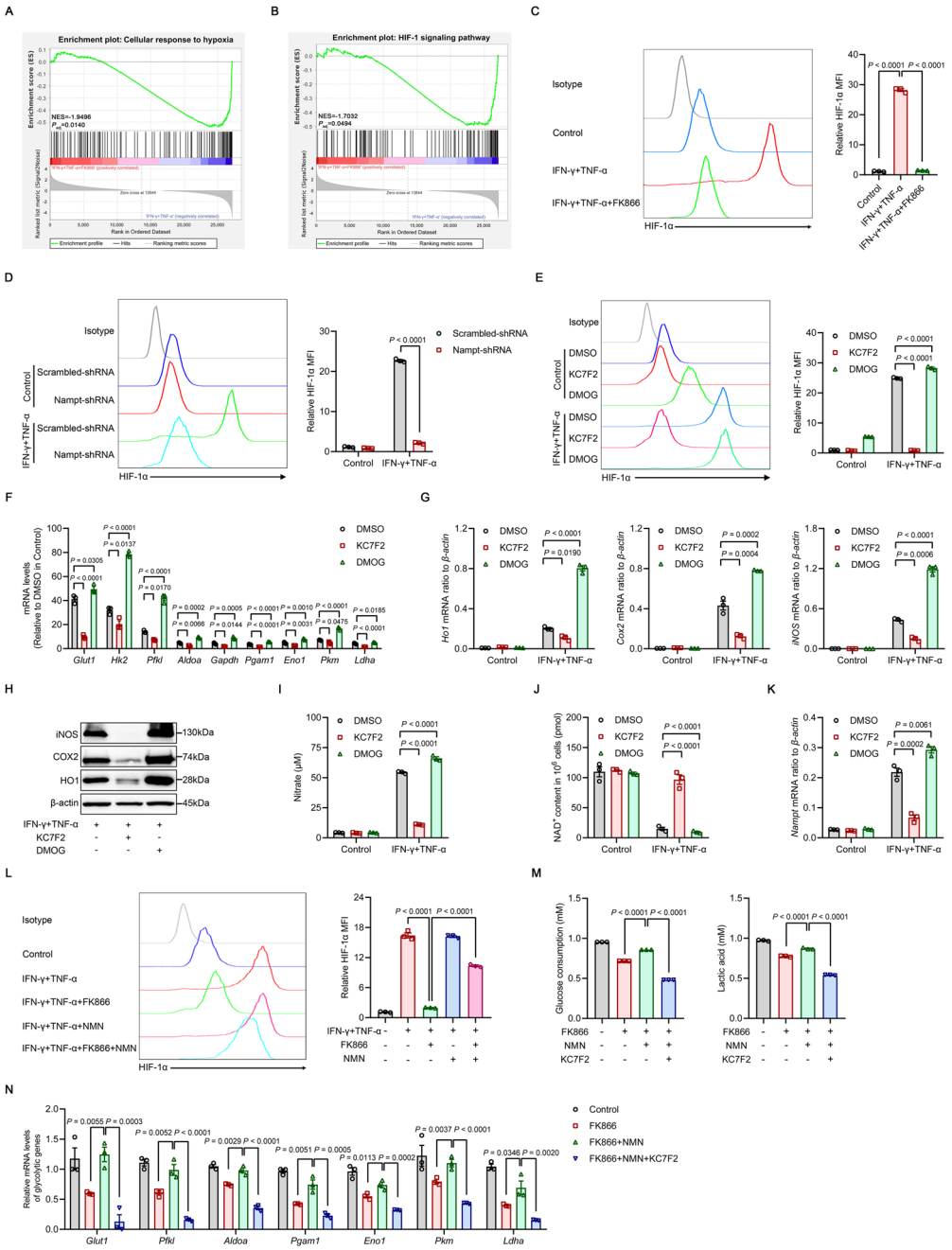

Fig. 6 HIF-1α mediates NAD^+-driven glycolysis in inflammatory cytokine-primed MSCs. **A**, **B** RNA-seq was performed on MSCs stimulated with IFN-γ and TNF-α (10 ng/ml each) for 24 h in the presence or absence of 50 nM FK866. The enrichment of genes in the cellular response to hypoxia was determined by GO enrichment analysis (**A**), and the HIF-1 signaling pathway was determined by KEGG enrichment analysis (**B**) and analyzed by GSEA. NES, normalized enrichment score; *P*adj, adjusted *P* value: two-tailed, corrected for multiple comparisons using the Benjamini–Hochberg method ($n = 3$). **C** HIF-1α expression was examined by flow cytometry in MSCs stimulated with IFN-γ and TNF-α (10 ng/ml each) for 24 h in the presence or absence of 50 nM FK866 ($n = 3$). **D** HIF-1α expression was examined by flow cytometry in MSCs transduced with Scrambled-shRNA or *Nampt*-shRNA and stimulated with IFN-γ and TNF-α (10 ng/ml each) for 24 h ($n = 3$). **E** HIF-1α expression was examined by flow cytometry in MSCs stimulated with IFN-γ and TNF-α (10 ng/ml each) for 24 h in the presence of 40 μM KC7F2 or 500 μM DMOG ($n = 3$). **F**, **G** The expression of glycolytic and immunomodulatory factors in MSCs stimulated with IFN-γ and TNF-α (10 ng/ml each) for 24 h in the presence of 40 μM KC7F2 or 500 μM DMOG was assayed by qRT–PCR ($n = 3$). **H** The expression of HO1, COX2, iNOS and β-actin (loading control) determined by immunoblotting in MSCs stimulated with IFN-γ and TNF-α (10 ng/ml each) for 24 h in the presence of 40 μM KC7F2 or 500 μM DMOG. **I** MSCs were stimulated with IFN-γ and TNF-α (10 ng/ml each) for 24 h in the presence of 40 μM KC7F2 or 500 μM DMOG, and the supernatants were assayed for nitrate by a modified Griess reagent ($n = 3$). **J** NAD^+ levels in MSCs stimulated with IFN-γ and TNF-α (10 ng/ml each) for 24 h in the presence of 40 μM KC7F2 or 500 μM DMOG ($n = 3$). **K** The expression of *Nampt* mRNA in MSCs stimulated with IFN-γ and TNF-α (10 ng/ml each) for 24 h in the presence of 40 μM KC7F2 or 500 μM DMOG was assayed by qRT–PCR ($n = 3$). **L** HIF-1α levels in MSCs stimulated with IFN-γ and TNF-α (10 ng/ml each) and treated with or without 50 nM FK866, 1 mM NMN or both FK866 and NMN for 24 h ($n = 3$). **M** Analysis of 24-h glucose consumption and lactate production in the supernatant of MSCs stimulated with IFN-γ and TNF-α (10 ng/ml each) with or without 50 nM FK866, 1 mM NMN or 40 μM KC7F2 for 24 h ($n = 3$). **N** The expression of glycolytic genes in MSCs stimulated with IFN-γ and TNF-α (10 ng/ml each) and the indicated combinations of 50 nM FK866, 1 mM NMN or 40 μM KC7F2 for 24 h was assayed by qRT–PCR ($n = 3$). MFI, mean fluorescence intensity. Values are presented as the mean ± SEM. Statistical analysis was performed by one-way analysis of variance

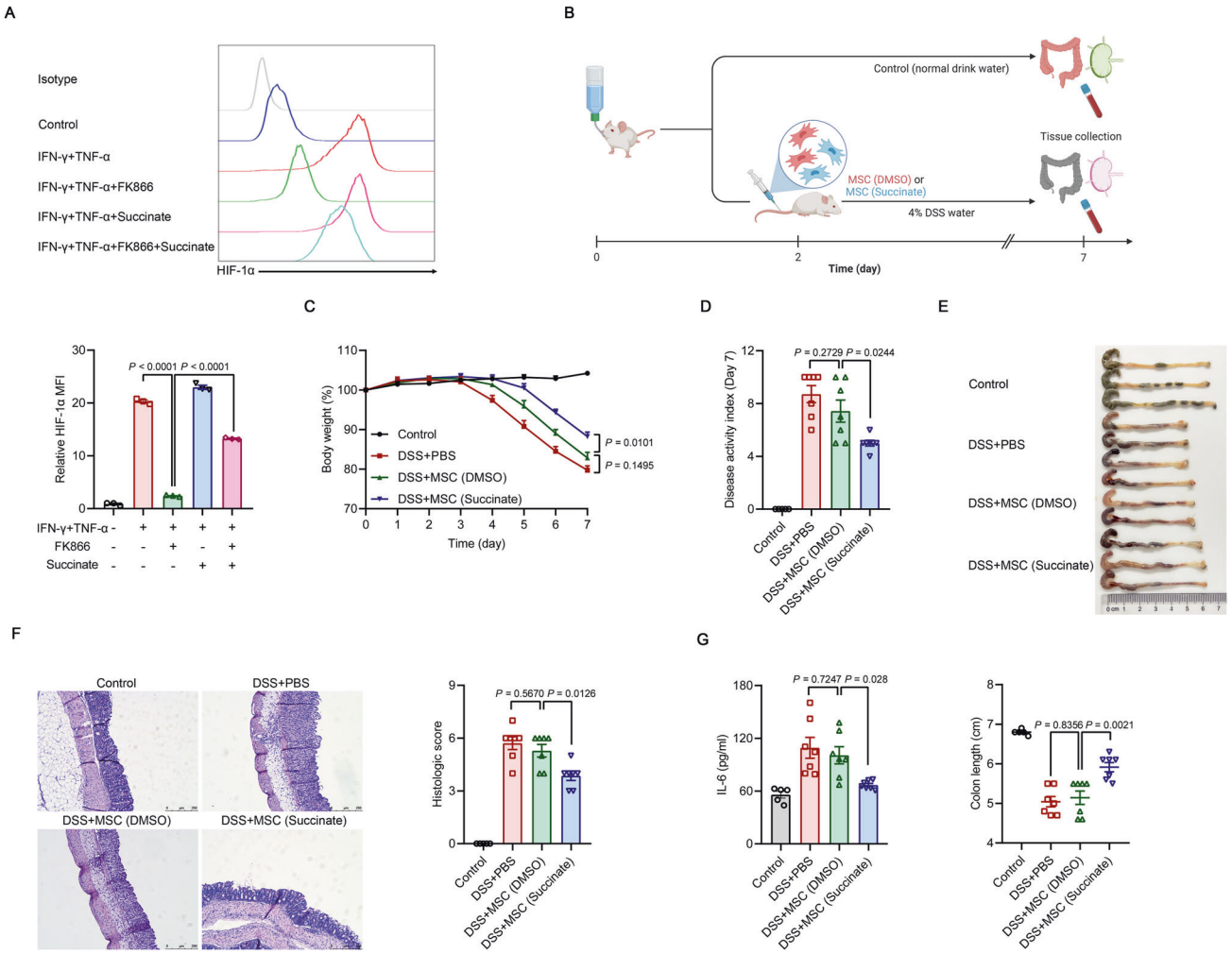

Fig. 7 Succinate drives HIF-1α-mediated immunomodulation in inflammatory cytokine-primed MSCs. **A** HIF-1α levels in MSCs stimulated with IFN-γ and TNF-α (10 ng/ml each) with or without 50 nM FK866 or 20 mM succinate for 24 h ($n = 3$). **B** Treatment of DSS-induced IBD by DMSO-pretreated MSCs or succinate-pretreated MSCs (1×10^5) administered intravenously to the mice on Day 2 after the beginning of DSS treatment. Mice in the control group received normal drinking water. On Day 7, the mice were euthanized, and the colons were excised. **C–E** Body weight, disease activity index and colon length of IBD mice administered DMSO-pretreated MSCs or succinate-pretreated MSCs. **F** Representative H&E-stained colon sections and histological scores of IBD mice that were administered DMSO-pretreated MSCs or succinate-pretreated MSCs. Scale bars, 250 μm. **G** IL-6 levels in the serum of IBD mice administered DMSO-pretreated MSCs or succinate-pretreated MSCs were assayed by ELISA (Control: $n = 5$, DSS + PBS: $n = 7$, DSS + MSC (DMSO): $n = 7$, DSS + MSC (Succinate): $n = 7$). MFI, mean fluorescence intensity. Values are presented as the mean ± SEM. Statistical analysis was performed by one-way analysis of variance

preclinical and clinical settings [1, 2, 4–6, 8, 57]. However, the immunomodulatory effects of MSCs are not constitutive but are activated and dictated by the type and intensity of inflammation. While MSCs cocultured with T cells without activation signals failed to inhibit T-cell proliferation, MSCs completely inhibited T-cell proliferation in response to a combination of IFN-γ plus TNF-α or IL-1, which are commonly released by activated T cells [9, 10]. These studies clearly demonstrated that MSC-mediated immunomodulation is highly plastic. In fact, hypoxic conditions can also affect the immunomodulatory phenotype of MSCs. Hypoxia-preconditioned MSCs exhibited stronger anti-inflammatory effects on experimental autoimmune encephalomyelitis (EAE) through the production of insulin-like growth factor 2 (IGF-2) [58]. Therefore, understanding the mechanisms governing the plasticity of MSC immunomodulation and developing more effective strategies for MSC-based therapeutic applications are highly desired in the clinic. Recent studies have revealed that metabolic reprogramming is essential for shaping the immunoregulatory properties of MSCs [37–39]. Given that NAD^+ acts as a cofactor to exert critical effects on energy generation from fuel substrates and is a cosubstrate for important NAD^+-consuming enzymes that determine cellular activation and stress responses [12–17], we hypothesized that NAD^+ metabolism could regulate the immunomodulatory function of MSCs in inflammatory microenvironments. Indeed, we found that NAD^+ pools were gradually depleted in inflammatory cytokine-primed MSCs compared to resting MSCs. Interestingly, NAD^+ depletion was coupled with the upregulation of NAMPT, which was essential for NAD^+ salvage in MSCs stimulated with IFN-γ and TNF-α, and the loss of NAMPT activity led to nearly complete NAD^+ depletion. These results indicate that the NAD^+ salvage pathway is indispensable for maintaining NAD^+ homeostasis in inflammatory cytokine-primed MSCs.

NAMPT, which converts NAM to NMN, is the first rate-limiting enzyme of the NAD^+ salvage pathway in mammals. Through its NAD^+-biosynthetic activity, NAMPT indirectly influences the functions of diverse NAD^+ catabolic enzymes, such as sirtuins, PARPs and cADPR synthetases, and thereby regulates cellular metabolism, mitochondrial biogenesis, redox regulation, DNA repair and inflammatory responses in various pathological

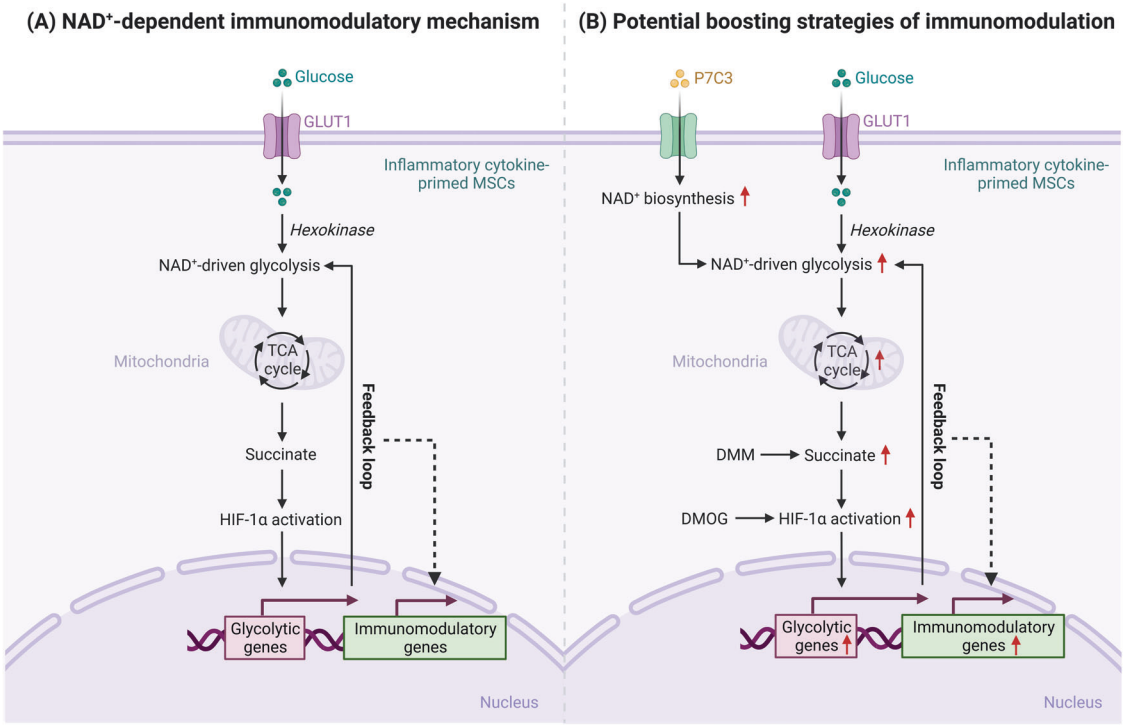

Fig. 8 A schematic model of NAD^+ metabolism-mediated immunomodulation in MSCs. **A** Inflammatory cytokine-primed MSCs rely on NAMPT in the NAD^+ salvage pathway to maintain intracellular NAD^+ pools, which are indispensable for glycolytic flux. The increase in glycolysis is accompanied by the accumulation of succinate, an intermediate metabolite of the mitochondrial tricarboxylic acid (TCA) cycle, which stabilizes the hypoxia-inducible factor-1α (HIF-1α) protein, increases glycolytic gene transcription and consequently shapes the NAD^+-dependent immunoregulatory properties of inflammatory cytokine-primed MSCs through this feedback loop. **B** Increasing NAD^+ biosynthesis by promoting NAMPT activity with P7C3 may be a novel strategy for optimizing the therapeutic efficacy of MSCs in inflammatory conditions. Moreover, enhancing succinate accumulation with DMM and increasing HIF-1α levels with DMOG are alternative approaches to elevating the immunoregulatory potential of inflammatory cytokine-primed MSCs

conditions and aging [12–17, 59]. Notably, we found that NAMPT inhibition or knockdown impaired the production of chemokines and inhibited the expression of immunomodulatory genes due to NAD^+ depletion in inflammatory cytokine-primed MSCs, and this effect could be rescued by the addition of NMN, the immediate NAD^+ precursor in the salvage pathway. Furthermore, the NAMPT activator P7C3 significantly enhanced the expression of various anti-inflammatory genes in MSCs stimulated with IFN-γ and TNF-α. Taken together, our data indicate that the immunomodulatory function of MSCs depends on the NAD^+ salvage pathway.

Increased NAMPT levels in immune cells are associated with various inflammatory disorders, including atherosclerosis, RA, GvHD and IBD [24, 60–62]. In preclinical studies, the NAMPT inhibitor FK866 effectively ameliorated experimental colitis in mice and dramatically decreased cytokine release from human lamina propria mononuclear cells in patients with IBD. Mechanistically, FK866-induced NAD^+ depletion skews proinflammatory macrophages toward anti-inflammatory phenotypes and antagonizes aberrant T-cell reactions [24, 62]. In contrast, an increase in NAMPT activity enhances NAD^+-dependent GAPDH activity, which is required for the Warburg effect in proinflammatory macrophages, and increases the production of inflammatory mediators, thus aggravating inflammatory conditions [63]. Therefore, targeting NAMPT in the NAD^+ salvage pathway is as a novel therapeutic approach for inflammatory disorders [12, 59]. However, this study showed that a lack of NAMPT activity impaired the immunomodulatory capability of MSCs, as indicated by the reduced inhibition of T-cell proliferation and anti-inflammatory polarization of macrophages, as well as the weakened therapeutic efficacy of MSCs in IBD and acute liver injury. Correspondingly, increasing NAMPT activity in MSCs with P7C3 enhanced their therapeutic potential in these disease models. The loss of NAMPT activity decreased the expression of key glycolytic genes, thereby lowering glycolytic rates and inhibiting the production of various glycolytic and TCA cycle intermediates. These findings in immune cells and MSCs indicated that the NAD^+ salvage pathway has distinct functions in different types of mammalian cells. While activated immune cells and primed MSCs rely on the NAD^+ salvage pathway to sustain glycolysis, they exert pro- and anti-inflammatory effects, respectively. Inflammatory macrophages rely on glycolysis to increase proinflammatory responses against invading pathogens [50]. In contrast, bioenergetic shifts toward aerobic glycolysis determine the immunosuppressive effect of inflammatory cytokine-primed MSCs [37, 38]. Therefore, NAMPT-dependent NAD^+ metabolism may lead to opposite outcomes in different types of mammalian cells to coordinately maintain tissue immune homeostasis and achieving a balance in the local microenvironment.

HIF-1α is critical for driving glycolysis in various immune cells in response to inflammatory stimulation, and it transactivates the expression of key glycolytic genes, such as *Glut1*, *Hk2*, *Pfkl*, *Aldoa*, *Gapdh*, *Pgam1*, *Eno1*, *Pkm* and *Ldha*, thereby allowing for sustained biosynthesis and ATP production [50, 64]. Our data showed that HIF-1α similarly transactivated glycolytic genes in inflammatory cytokine-primed MSCs and conferred immunosuppressive properties, which was consistent with a previous study [65]. The TCA cycle intermediate succinate accumulates in inflammatory macrophages following LPS treatment. Excessive cytosolic succinate is transported from the mitochondria and suppresses the catalytic activity of PHD, thereby promoting the stabilization of HIF-1α protein, which then activates the transcription of a number of genes, including genes encoding

proinflammatory cytokines, as well as those involved in glycolytic enzymes [54, 55]. DMOG can inhibit the hydroxylation activity of PHD, thus stabilizing the HIF-1α protein [52]. DMOG further enhances the expression of HIF-1α-targeted glycolytic genes and subsequent anti-inflammatory gene levels, suggesting that PHD inhibition promotes HIF-1α activity in inflammatory cytokine-primed MSCs. Similarly, supplementation with succinate, an important negative regulator of PHD, partially rescued the decrease in glycolytic activity and consequently restored the immunomodulatory ability of MSCs with NAMPT loss of function, suggesting that the circuitry consisting of succinate accumulation, HIF-1α stabilization and glycolysis adequately sustains the expression of immunoregulatory factors in inflammatory cytokine-primed MSCs only when there is a constant supply of NAD^+ that is supported by the NAMPT-mediated salvage pathway. However, this rescue effect of succinate was abrogated by the HIF-1α inhibitor KC7F2, suggesting that succinate is a crucial intermediate metabolite in HIF-1α-mediated immunomodulation of inflammatory cytokine-primed MSCs. In addition, increasing succinate accumulation in the cytosol with DMM significantly elevated glycolytic rates and enhanced the expression of immunomodulatory genes. More importantly, preconditioning with succinate improved the immunoregulatory properties and therapeutic efficacy of MSCs in the IBD model. Thus, our findings show that priming MSCs with metabolites represents a promising strategy to increase MSC therapeutic efficacy in diseases.

Although this study reveals that the decrease in NAD^+ is attributed to increased catabolic activity, such as glycolysis and the TCA cycle, the role of NAD^+ degradation enzymes, including PARP1, CD38 and SIRTs, in NAD^+ consumption in inflammatory cytokine-primed MSCs remains unknown. In addition, the mechanism underlying the up- or downregulation of NAMPT in response to NAD^+ availability in MSCs after inflammatory stimulation remains unclear. This study delineated the role of NAD^+ metabolism in shaping the immunoregulatory properties of inflammatory cytokine-primed MSCs, but it is still unclear how NAD^+ dynamics determine the immunomodulatory activity of MSCs due to the lack of a method for manipulating NAD^+ levels in MSCs in situ. This is a fundamental question that needs to be solved in the future.

Collectively, our work identified an NAD^+ salvage-based mechanism underlying the immunoregulatory functions of MSCs. Inflammatory cytokine-primed MSCs rely on NAMPT to maintain NAD^+ pools, which are indispensable for driving glycolysis. Cytosolic succinate accumulation following the increases in glycolysis and the TCA cycle can stabilize the HIF-1α protein and subsequently increase the transcription of key glycolytic genes, thereby sustaining glycolytic activity and shaping the immunoregulatory properties of inflammatory cytokine-primed MSCs through this feedback loop (Fig. 8). These findings illustrate distinct roles of NAD^+ metabolism in different types of mammalian cells and provide novel modalities for better therapeutic applications of MSCs in inflammatory diseases.

REFERENCES

1. Uccelli A, Moretta L, Pistoia V. Mesenchymal stem cells in health and disease. Nat Rev Immunol. 2008;8:726–36.
2. Shi Y, Su J, Roberts AI, Shou P, Rabson AB, Ren G. How mesenchymal stem cells interact with tissue immune responses. Trends Immunol. 2012;33:136–43.
3. Shi Y, Hu G, Su J, Li W, Chen Q, Shou P, et al. Mesenchymal stem cells: a new strategy for immunosuppression and tissue repair. Cell Res. 2010;20:510–518.
4. Wang Y, Chen X, Cao W, Shi Y. Plasticity of mesenchymal stem cells in immunomodulation: pathological and therapeutic implications. Nat Immunol. 2014;15:1009–16.
5. Shi Y, Du L, Lin L, Wang Y. Tumour-associated mesenchymal stem/stromal cells: emerging therapeutic targets. Nat Rev Drug Discov. 2017;16:35–52.
6. Shi Y, Wang Y, Li Q, Liu K, Hou J, Shao C, et al. Immunoregulatory mechanisms of mesenchymal stem and stromal cells in inflammatory diseases. Nat Rev Nephrol. 2018;14:493–507.
7. Krampera M, Le Blanc K. Mesenchymal stromal cells: Putative microenvironmental modulators become cell therapy. Cell Stem Cell. 2021;28:1708–25.
8. Wang Y, Fang J, Liu B, Shao C, Shi Y. Reciprocal regulation of mesenchymal stem cells and immune responses. Cell Stem Cell. 2022;29:1515–30.
9. Ren G, Zhang L, Zhao X, Xu G, Zhang Y, Roberts AI, et al. Mesenchymal stem cell-mediated immunosuppression occurs via concerted action of chemokines and nitric oxide. Cell Stem Cell. 2008;2:141–50.
10. Su J, Chen X, Huang Y, Li W, Li J, Cao K, et al. Phylogenetic distinction of iNOS and IDO function in mesenchymal stem cell-mediated immunosuppression in mammalian species. Cell Death Differ. 2014;21:388–96.
11. Nemeth K, Leelahavanichkul A, Yuen PS, Mayer B, Parmelee A, Doi K, et al. Bone marrow stromal cells attenuate sepsis via prostaglandin E(2)-dependent reprogramming of host macrophages to increase their interleukin-10 production. Nat Med. 2009;15:42–49.
12. Garten A, Schuster S, Penke M, Gorski T, de Giorgis T, Kiess W. Physiological and pathophysiological roles of NAMPT and NAD metabolism. Nat Rev Endocrinol. 2015;11:535–46.
13. Rajman L, Chwalek K, Sinclair DA. Therapeutic Potential of NAD-Boosting Molecules: The In Vivo Evidence. Cell Metab. 2018;27:529–47.
14. Ralto KM, Rhee EP, Parikh SM. NAD(+) homeostasis in renal health and disease. Nat Rev Nephrol. 2020;16:99–111.
15. Xie N, Zhang L, Gao W, Huang C, Huber PE, Zhou X, et al. NAD(+) metabolism: pathophysiologic mechanisms and therapeutic potential. Signal Transduct Target Ther. 2020;5:227.
16. Covarrubias AJ, Perrone R, Grozio A, Verdin E. NAD(+) metabolism and its roles in cellular processes during ageing. Nat Rev Mol Cell Biol. 2021;22:119–41.
17. Chini CCS, Zeidler JD, Kashyap S, Warner G, Chini EN. Evolving concepts in NAD(+) metabolism. Cell Metab. 2021;33:1076–87.
18. Fang J, Chen W, Hou P, Liu Z, Zuo M, Liu S, et al. NAD(+) metabolism-based immunoregulation and therapeutic potential. Cell Biosci. 2023;13:81.
19. Evans J, Wang TC, Heyes MP, Markey SP. LC/MS analysis of NAD biosynthesis using stable isotope pyridine precursors. Anal Biochem. 2002;306:197–203.
20. Revollo JR, Grimm AA, Imai S. The NAD biosynthesis pathway mediated by nicotinamide phosphoribosyltransferase regulates Sir2 activity in mammalian cells. J Biol Chem. 2004;279:50754–63.
21. Yang H, Yang T, Baur JA, Perez E, Matsui T, Carmona JJ, et al. Nutrient-sensitive mitochondrial NAD+ levels dictate cell survival. Cell. 2007;130:1095–107.
22. Muraoka H, Hasegawa K, Sakamaki Y, Minakuchi H, Kawaguchi T, Yasuda I, et al. Role of Nampt-Sirt6 Axis in Renal Proximal Tubules in Extracellular Matrix Deposition in Diabetic Nephropathy. Cell Rep. 2019;27:199–212.e195.
23. Zhang LQ, Van Haandel L, Xiong M, Huang P, Heruth DP, Bi C, et al. Metabolic and molecular insights into an essential role of nicotinamide phosphoribosyltransferase. Cell Death Dis. 2017;8:e2705.
24. Gerner RR, Klepsch V, Macheiner S, Arnhard K, Adolph TE, Grander C, et al. NAD metabolism fuels human and mouse intestinal inflammation. Gut 2018;67:1813–23.
25. Han X, Yang Q, Lin L, Xu C, Zheng C, Chen X, et al. Interleukin-17 enhances immunosuppression by mesenchymal stem cells. Cell Death Differ. 2014;21:1758–68.
26. Li X, Shang B, Li YN, Shi Y. Shao C. IFNgamma and TNFalpha synergistically induce apoptosis of mesenchymal stem/stromal cells via the induction of nitric oxide. Stem Cell Res Ther. 2019;10:18.
27. Miranda KM, Espey MG, Wink DA. A rapid, simple spectrophotometric method for simultaneous detection of nitrate and nitrite. Nitric Oxide. 2001;5:62–71.
28. Fang J, Zhang S, Liu Z, Pan Y, Cao L, Hou P, et al. Skeletal muscle stem cells confer maturing macrophages anti-inflammatory properties through insulin-like growth factor-2. Stem Cells Transl Med. 2020;9:773–85.
29. Verdin E. NAD(+) in aging, metabolism, and neurodegeneration. Science. 2015;350:1208–13.
30. Imai S, Guarente L. NAD+ and sirtuins in aging and disease. Trends Cell Biol. 2014;24:464–71.
31. Katsyuba E, Romani M, Hofer D, Auwerx J. NAD(+) homeostasis in health and disease. Nat Metab. 2020;2:9–31.
32. Grahnert A, Grahnert A, Klein C, Schilling E, Wehrhahn J, Hauschildt S. Review: NAD+: a modulator of immune functions. Innate Immun. 2011;17:212–33.
33. Minhas PS, Liu L, Moon PK, Joshi AU, Dove C, Mhatre S, et al. Macrophage de novo NAD(+) synthesis specifies immune function in aging and inflammation. Nat Immunol. 2019;20:50–63.
34. Billingham LK, Chandel NS. NAD-biosynthetic pathways regulate innate immunity. Nat Immunol. 2019;20:380–82.
35. Navarro MN, Gomez de Las Heras MM, Mittelbrunn M. Nicotinamide adenine dinucleotide metabolism in the immune response, autoimmunity and inflammageing. Br J Pharmacol. 2022;179:1839–56.
36. Navas LE, Carnero A. NAD(+) metabolism, stemness, the immune response, and cancer. Signal Transduct Target Ther. 2021;6:2.

37. Jitschin R, Bottcher M, Saul D, Lukassen S, Bruns H, Loschinski R, et al. Inflammation-induced glycolytic switch controls suppressivity of mesenchymal stem cells via STAT1 glycosylation. Leukemia. 2019;33:1783–96.
38. Contreras-Lopez R, Elizondo-Vega R, Luque-Campos N, Torres MJ, Pradenas C, Tejedor G, et al. The ATP synthase inhibition induces an AMPK-dependent glycolytic switch of mesenchymal stem cells that enhances their immunotherapeutic potential. Theranostics. 2021;11:445–60.
39. Xu C, Feng C, Huang P, Li Y, Liu R, Liu C, et al. TNFalpha and IFNgamma rapidly activate PI3K-AKT signaling to drive glycolysis that confers mesenchymal stem cells enhanced anti-inflammatory property. Stem Cell Res Ther. 2022;13:491.
40. Hasmann M, Schemainda I. FK866, a highly specific noncompetitive inhibitor of nicotinamide phosphoribosyltransferase, represents a novel mechanism for induction of tumor cell apoptosis. Cancer Res. 2003;63:7436–42.
41. Yoshino J, Baur JA, Imai SI. NAD(+) Intermediates: The Biology and Therapeutic Potential of NMN and NR. Cell Metab. 2018;27:513–28.
42. Pieper AA, Xie S, Capota E, Estill SJ, Zhong J, Long JM, et al. Discovery of a proneurogenic, neuroprotective chemical. Cell 2010;142:39–51.
43. Wang G, Han T, Nijhawan D, Theodoropoulos P, Naidoo J, Yadavalli S, et al. P7C3 neuroprotective chemicals function by activating the rate-limiting enzyme in NAD salvage. Cell. 2014;158:1324–34.
44. Na YR, Stakenborg M, Seok SH, Matteoli G. Macrophages in intestinal inflammation and resolution: a potential therapeutic target in IBD. Nat Rev Gastroenterol Hepatol. 2019;16:531–43.
45. Dieleman LA, Ridwan BU, Tennyson GS, Beagley KW, Bucy RP, Elson CO. Dextran sulfate sodium-induced colitis occurs in severe combined immunodeficient mice. Gastroenterology. 1994;107:1643–52.
46. Krieglstein CF, Cerwinka WH, Sprague AG, Laroux FS, Grisham MB, Koteliansky VE, et al. Collagen-binding integrin alpha1beta1 regulates intestinal inflammation in experimental colitis. J Clin Investig. 2002;110:1773–82.
47. Xiao YT, Yan WH, Cao Y, Yan JK, Cai W. Neutralization of IL-6 and TNF-alpha ameliorates intestinal permeability in DSS-induced colitis. Cytokine. 2016;83:189–92.
48. Wang H, Feng X, Yan W, Tian D. Regulatory T Cells in Autoimmune Hepatitis: Unveiling Their Roles in Mouse Models and Patients. Front Immunol. 2020;11:575572.
49. Luengo A, Li Z, Gui DY, Sullivan LB, Zagorulya M, Do BT, et al. Increased demand for NAD(+) relative to ATP drives aerobic glycolysis. Mol Cell. 2021;81:691–707. e696.
50. Kelly B, O'Neill LA. Metabolic reprogramming in macrophages and dendritic cells in innate immunity. Cell Res. 2015;25:771–84.
51. Liu R, Li X, Ma H, Yang Q, Shang Q, Song L, et al. Spermidine endows macrophages anti-inflammatory properties by inducing mitochondrial superoxide-dependent AMPK activation, Hif-1alpha upregulation and autophagy. Free Radic Biol Med. 2020;161:339–50.
52. Zhou B, Ge T, Zhou L, Jiang L, Zhu L, Yao P, et al. Dimethyloxalyl Glycine Regulates the HIF-1 Signaling Pathway in Mesenchymal Stem Cells. Stem Cell Rev Rep. 2020;16:702–10.
53. Selak MA, Armour SM, MacKenzie ED, Boulahbel H, Watson DG, Mansfield KD, et al. Succinate links TCA cycle dysfunction to oncogenesis by inhibiting HIF-alpha prolyl hydroxylase. Cancer Cell. 2005;7:77–85.
54. Tannahill GM, Curtis AM, Adamik J, Palsson-McDermott EM, McGettrick AF, Goel G, et al. Succinate is an inflammatory signal that induces IL-1beta through HIF-1alpha. Nature. 2013;496:238–42.
55. Wen H, Ting JP. Agitation by suffocation: how hypoxia activates innate immunity via the Warburg effect. Cell Metab. 2013;17:814–15.
56. Mills EL, Kelly B, Logan A, Costa ASH, Varma M, Bryant CE, et al. Succinate Dehydrogenase Supports Metabolic Repurposing of Mitochondria to Drive Inflammatory Macrophages. Cell. 2016;167:457–70.e413.
57. Fang J, Feng C, Chen W, Hou P, Liu Z, Zuo M, et al. Redressing the interactions between stem cells and immune system in tissue regeneration. Biol Direct. 2021;16:18.
58. Du L, Lin L, Li Q, Liu K, Huang Y, Wang X, et al. IGF-2 Preprograms Maturing Macrophages to Acquire Oxidative Phosphorylation-Dependent Anti-inflammatory Properties. Cell Metab. 2019;29:1363–75.e1368.
59. Audrito V, Messana VG. Deaglio S. NAMPT and NAPRT: Two Metabolic Enzymes With Key Roles in Inflammation. Front Oncol. 2020;10:358.
60. Kim D, Lee G, Huh YH, Lee SY, Park KH, Kim S, et al. NAMPT Is an Essential Regulator of RA-Mediated Periodontal Inflammation. J Dent Res. 2017;96:703–11.
61. Kong YY, Li GQ, Zhang WJ, Hua X, Zhou CC, Xu TY, et al. Nicotinamide phosphoribosyltransferase aggravates inflammation and promotes atherosclerosis in ApoE knockout mice. Acta Pharm Sin. 2019;40:1184–92.
62. Gerner RR, Macheiner S, Reider S, Siegmund K, Grabherr F, Mayr L, et al. Targeting NAD immunometabolism limits severe graft-versus-host disease and has potent antileukemic activity. Leukemia 2020;34:1885–97.
63. Cameron AM, Castoldi A, Sanin DE, Flachsmann LJ, Field CS, Puleston DJ, et al. Inflammatory macrophage dependence on NAD(+) salvage is a consequence of reactive oxygen species-mediated DNA damage. Nat Immunol. 2019;20:420–32.
64. Corcoran SE, O'Neill LA. HIF1alpha and metabolic reprogramming in inflammation. J Clin Investig. 2016;126:3699–707.
65. Contreras-Lopez R, Elizondo-Vega R, Paredes MJ, Luque-Campos N, Torres MJ, Tejedor G, et al. HIF1alpha-dependent metabolic reprogramming governs mesenchymal stem/stromal cell immunoregulatory functions. FASEB J. 2020;34:8250–64.

ACKNOWLEDGEMENTS

This study was supported by grants from the National Key R&D Program of China (2021YFA1100600 and 2022YFA0807300), the National Natural Science Foundation of China (82202032, 81930085 and 32150710523), the Jiangsu Province International Joint Laboratory for Regenerative Medicine Fund and the Suzhou Foreign Academician Workstation Fund (SWY202202).

AUTHOR CONTRIBUTIONS

JF: conception and design, collection and assembly of data, animal experiments, data analysis and interpretation, and manuscript writing. PH, SL, MZ, ZL, WC and CF: conception and design, data analysis and interpretation. YH, YL and TW: data analysis and interpretation. WC and CF: animal experiments. PL: data analysis and interpretation. CS and YS: conception and design, manuscript writing, administrative support and financial support.

COMPETING INTERESTS

The authors declare no competing interests.

ADDITIONAL INFORMATION

Supplementary information The online version contains supplementary material available at https://doi.org/10.1038/s41423-023-01073-2.

Correspondence and requests for materials should be addressed to Changshun Shao or Yufang Shi.